Copy No. 8

DEFENCE R&D DÉFENSE

THEORETICAL MANUAL FOR **SEALOADS**: A THREE-DIMENSIONAL NONLINEAR TIME-DOMAIN SEA LOADS COMPUTER CODE

L.Cong – W.Qiu – C.C.Hsiung

Centre for Marine Vessel Development and Research
DalTech
Dalhousie University
P.O. Box 1000, Halifax, Nova Scotia, B3J 2X4

DEFENCE RESEARCH ESTABLISHMENT ATLANTIC

Contractor Report

DREA CR/98/443

October 1999

National Defence Défense nationale

Canada

National Defence
Research and Development Branch

Défense nationale
Bureau de recherche et développement

DREA CR/98/443

Theoretical Manual for **SEALOADS**:

A Three-Dimensional Nonlinear Time-Domain Sea Loads Computer Code

L.Cong – W.Qiu – C.C.Hsiung

Centre for Marine Vessel Development and Research
DalTech
P.O. Box 1000, Halifax, NS B3J 2X4

Scientific Authority S.Ando

W7707-7-4636
Contract Number

October 1999

CONTRACTOR REPORT

Prepared for

Defence Research Establishment Atlantic

Centre de Recherches pour la Défense Atlantique

Canada

102-00737/

Report on

Theoretical Manual for SEALOADS: A Three-Dimensional Nonlinear Time-Domain Sea Loads Computer Code

Prepared for the Defence Research Establishment Atlantic
Department of National Defence
Dartmouth, Nova Scotia
Contract No. W7707-7-4636/001/HAL

by

Liangzi Cong, Wei Qiu and C. C. Hsiung

Centre for Marine Vessel Development and Research
DalTech
Dalhousie University
P.O. Box 1000, Halifax, Nova Scotia, B3J 2X4

October 1999

ABSTRACT

This report describes the theoretical formulation for SEALOADS, a computer program for the time-domain prediction of ship motions, sea loads, and hydrodynamic pressures on a ship hull. The three-dimensional time-domain Green function is used to derive the forces due to radiated and diffracted waves. The Froude-Krylov forces are computed at the instantaneous position using the three-dimensional panel method. Nonlinear viscous damping, resistance, and cross-flow drag are included. The propeller thrust, rudder and maneuvering forces are also taken into account. After the nonlinear equations of ship motions are solved in the time domain, hydrodynamic pressures on the ship hull and bending moments and shear forces acting on a cross section of the ship are computed.

RÉSUMÉ

Le présent rapport décrit la formulation théorique de SEALOADS, programme informatique qui permet de prédire, dans le domaine temporel, les mouvements d'un navire, les charges de mer et les pressions hydrodynamiques exercées sur la coque d'un navire. La fonction tridimensionnelle de Green dans le domaine temporel permet de déterminer les forces dues aux effets de rayonnement et de diffraction des vagues. Les forces de Froude-Krylov sont calculées à la position instantanée au moyen de la méthode des panneaux tridimensionnels. L'amortissement visqueux non linéaire, la résistance et la traînée due à l'écoulement transversal sont compris. La poussée de l'hélice et les forces de gouvernail et de manœuvre sont aussi prises en compte. Une fois que les équations non linéaires des mouvements du navire sont résolues dans le domaine temporel, les pressions hydrodynamiques exercées sur la coque du navire, le moment de flexion et les forces de cisaillement agissant sur la section transversale du navire sont calculés.

Contents

Abstract ii

List of Figures v

Nomenclature vii

1 Introduction 1

1.1 Basic Features 1

1.2 Literature Review 2

2 Nonlinear Ship Motion in the Time Domain 4

2.1 Equations of Ship Motion 4

2.2 Nonlinear Froude-Krylov Forces 6

2.3 Viscous Forces and Moments 8

2.3.1 Viscous Roll Damping 8

2.3.2 Resistance 8

2.3.3 Cross-Flow Drag 9

2.4 Propeller Thrust 9

2.5 Maneuvering Forces 9

2.6 Rudder Forces and Autopilot 10

3 Forces due to the Radiated and Diffracted Waves 11

3.1 Solutions of the Radiated Wave Potentials 11

3.2 Forces due to the Radiated Waves 13

3.3 Forces due to Diffracted Waves 22

4 Code Structure of SEALOADS 26

5 Pressure on Ship Hull 31

5.1 Pressure induced by incident waves 31
5.2 Pressure induced by radiated waves 31
5.3 Pressure induced by diffracted waves 33

6 Sea Loads 35

7 Conclusions 36

Appendix A: The Radiation and Diffraction Problems 37

Appendix B: The Time-Domain Green Function 43

Appendix C: Numerical Solutions of the Potential Functions 48

Appendix D: Results of Roll Damping for Series 60 Hull 50

Appendix E: Numerical Results 52

References 63

List of Figures

1 Coordinate Systems for Ship Motions 4

2 Panelization of a Hemi-sphere 16

3 Response function $K_{33}(t)$ of a hemisphere ($F_n = 0$) 17

4 Added mass and damping coefficient of a hemisphere ($F_n = 0$) 18

5 Panelization of a Series 60 (C_B=0.7) 19

6 Response function $K_{33}(t)$ of a Series 60, $C_B = 0.7$ ($F_n = 0$) 20

7 Added mass and damping coefficient for Series 60, $C_B = 0.7$ ($F_n = 0$) 21

8 Response function $K_{27}(t)$ and $K_{37}(t)$ for a hemisphere ($F_n = 0$) 25

9 Main Modules of SEALOADS 27

10 Flow Chart of Radiation Module 28

11 Flow Chart of Diffraction Module 29

12 Flow Chart of Motion, Pressure and Seaload Module 30

13 Body Plan of Series 60, C_B=0.70. 50

14 Panelized Hull of Series 60, C_B=0.70. 50

15 Computed Viscous Roll Damping, $F_n = 0.2$. 51

16 Fitted Roll Damping based on Fig.15. 51

17 Panelization of CPF hull 52

18 Raw and Smoothed Data of Pressure of CPF model (V_s=3.4 knot) 54

19 Raw and Smoothed Data of Shear Force of CPF model (V_s=3.4 knot) 55

20 Raw and Smoothed Data of Bending Moment of CPF model (V_s=3.4 knot) . 56

21 Wave, Motions and Sealoads of CPF at V_s=3.4 knot (— SEALOADS - - - Experiment) 57

22 Hull Pressure on CPF (V_s=3.4 knot) 58

23 Wave, Motions and Sealoads of CPF (V_s=8.2 knot) 59

24 Hull Pressure on CPF (V_s=8.2 knot) 60

25 Wave, Motions and Sealoads of CPF (V_s=12 knot) 61

26 Hull Pressure on CPF (V_s=12 knot) 62

Nomenclature

α_1^ν, α_2^ν	the linear-quadratic viscous roll damping coefficients
α_1^r	the yaw gain
α_2^r	the yaw rate gain
Γ	contour of the mean waterline
$\bar{\gamma}_{kj}$	coefficient of time domain hydrodynamic restoring force
δ	rudder angle
δ_0	the threshold value of yaw beyond which the rudder is activated
δ_e	the effective rudder angle
ζ_0	wave profile
$\eta_j(t)$	small amplitude motion of the ship in the j^{th} mode
λ	the wave length
$\bar{\lambda}$	the aspect ratio of the rudder
$\bar{\lambda_{kj}}$	time domain hydrodynamic damping
$\bar{\mu}_{kj}$	time domain added mass
ξ_1, ξ_2, ξ_3	the displacements of the centre of gravity
ρ	water density
σ	source strength
$\bar{\Phi}$	velocity potential of steady flow around the ship hull
ϕ_j	velocity potential of radiated waves
φ_j	velocity potential of radiated waves due to impulsive ship motion
χ_j	function due to impulsive displacement of the ship
ψ_j	function due to impulsive velocity of the ship
ω	incident wave frequency
ω_e	frequency of encounter

A_r	the rudder area of a single side
$C_d(x_s)$	the sectional cross-flow drag coefficient
d	the ship draft
D_p	the propeller diameter
e_1, e_2, e_3	the Eulerian angles between the $o_s x_s y_s z_s$ and the $o_m x_m y_m z_m$
F_I	inertial force components
F_k^V	viscous forces including viscous roll damping moment, resistance and cross-flow drag
F_k^{Dif}	the diffracted wave forces
F_k^{FK}	nonlinear Froude-Krylov forces
F_k^H	the hull maneuvering forces
F_k^{Prop}	the propeller thrust
F_k^{Rad}	the radiated wave forces
F_k^{Rs}	the restoring forces
F_k^{Rud}	the rudder force
F_P	forces including all other hydrodynamic components
F_S	vertical shear force
G	Green function
g	acceleration of gravity
H	the wave height
I_{11}	moment of inertia of roll of a ship
I_{22}	moment of inertia of pitch of a ship
I_{33}	moment of inertia of yaw of a ship
I_{kj}	product of inertia of a ship
J	the advancing coefficient
K_Q	the torque coefficient

K_T	the thrust coefficient
$K_{ij}(t)$	the memory function
L	ship length
l_x	horizontal distances between the pressure point C_{rud} and the centre of gravity
l_z	vertical distances between the pressure point C_{rud} and the centre of gravity
m	ship mass
M_B	vertical bending moment
M_I	inertial moment components
m_j	m_j-terms
M_P	moments including all other hydrodynamic components
m_{cx}	the mass of the portion of the ship between the bow and the cross section x_c
n_p	the revolution per second
n_{kj}	the k^{th} component of the unit normal on the j^{th} panel
$o_m x_m y_m z_m$	The moving coordinate system
$o_s x_s y_s z_s$	The coordinate system fixed on the ship
OXY	The spaced-fixed coordinate system
P	the pressure
p_i	the pressure at a nodal point of the panel
P_d	dynamic pressure
$p_d(P,t)$	the pressure due to diffracted waves
$p_i(P,t)$	the pressure due to incident waves
$p_r(P,t)$	the pressure due to radiated waves
P_s	static pressure
$\bar{P}$	mean pressure

r_{xx}	the radius of gyration of the portion of the ship forward of x_c
S_F	the surface of the hull between the bow and the cross section at x_c
$S_{\zeta\zeta}$	wave spectrum
$\bar{S}$	mean wetted surface of ship hull
ΔS_j	the area of the j^{th} panel
t	time
$T(x_s)$	the local draft of the ship
t_p	the thrust deduction fraction
U	the steady forward speed of the ship
u_1, u_2, u_3	translational velocities of a ship in $o_s x_s y_s z_s$
u_4, u_5, u_6	rotational velocities of a ship in $o_s x_s y_s z_s$
U_{cx}	longitudinal components of current
U_{cy}	lateral components of current
$v_2(x_s, t)$	the transverse relative velocity between the hull and the water particle of the local cross-flow
V_r	the relative velocity of the water particle to the rudder
V_s	ship speeds
$\vec{W}$	the disturbance velocity due to the steady forward speed of the ship
x_g and x_G	the x coordinates of the centres of gravity of the ship segment forward of x_c and of the whole ship
x_p	the x coordinate of the hull point P
x_{sg}, y_{sg}, z_{sg}	the coordinates of the centre of gravity of the ship in the ship-fixed coordinate system

1 Introduction

This report describes the theoretical background of a three-dimensional nonlinear Time-Domain Sea Loads Computer Program, **SEALOADS**, for the Department of National Defence. This work has been carried out at the Centre for Marine Vessel Development and Research (CMVDR), DalTech, Dalhousie University (formerly the Technical University of Nova Scotia).

1.1 Basic Features

A computer software package called NOSMA (Huang and Hsiung 1996, Huang et al. 1998) has been developed for the past four years at CMVDR to predict the large-amplitude ship motions up to the point of capsize. NOSMA has been validated for fishing vessels (Huang et al., 1996) and applied to predict ship capsizing in extreme seas. In NOSMA, the frequency-domain damping coefficients are transformed to compute the memory functions, and diffracted wave forces in the frequency domain are converted in the time-domain ship motion computation.

According to the requirements of this project, the time-domain Green function is to be used for the forces due to radiated and diffracted waves as a substitute for the corresponding force components in NOSMA. Moreover, the computation of pressure distribution on the ship hull, which is not dealt with in NOSMA, is an important requirement in order to provide the hydrodynamic loading for the hydroelastic analysis of a ship in waves. Thus, the methodology has to be improved for the time-domain analysis. The new code, SEALOADS, with such enhancement and improvement, is developed with the following features:

- the time-domain added mass, hydrodynamic restoring force, and damping force coefficients are computed using the impulse potential function (linear);
- the forces due to the radiated and diffracted waves are computed based on the time-domain analysis in terms of the response function method (linear);
- Froude-Krylov and buoyancy forces are computed at the instantaneous position using the 3-D panel method (nonlinear);
- viscous damping, resistance, cross-flow drag are included (nonlinear);
- propeller thrust, rudder and maneuvering forces are included (nonlinear);
- nonlinear equations of ship motion are solved in the time domain; and
- the hydrodynamic pressures distributed on the ship hull and the sea loads acting on a cross section of the ship are also computed.

1.2 Literature Review

The time-domain hydrodynamic forces can be directly computed in the time domain or indirectly converted from the frequency-domain added masses and damping coefficients. Applications based on the frequency-domain hydrodynamic coefficients can be found in papers by van Oortmerssen (1976), and de Kat and Paulling (1989). In a more direct application of strip theory to the prediction of large-amplitude ship motions and loads in the time domain, the radiation and diffraction forces are calculated in terms of frequency-dependent sectional added-mass and damping coefficients. However, the strip-theory approach is inadequate for calculating hydrodynamic pressure distributions on the hull, which are necessary for structural analyses concerning grillages, panels, and plates. As a result, the three-dimensional method must be used.

Based on the methods introduced by Cummins (1962) and Wehausen (1967), the time-domain ship motion can be solved directly by using the time-domain Green function derived by Finklestein (1957). The advantages of the direct method are that it can be extended to solve the quasi-nonlinear hydrodynamic problem as shown by Lin and Yue (1990). Moreover, it is easier to compute the time-domain Green function numerically than to compute the frequency-domain counterpart with a forward speed. For the application of the three-dimensional time-domain Green function to the radiation and diffraction problems for ships with or without forward speed, many works have been published, such as Liapis and Beck (1985), Beck and Liapis (1987), Beck and King (1989), Beck and Magee (1990) and Lin and Yue (1994).

Lin and Yue (1990, 1994) gave the report on the large-amplitude ship motions and sea loads in the time domain. The differences between Lin and Yue's work and the earlier work by others using the linear time-domain approximation are that, in the former, the wetted surface of the ship hull is re-panelized at each time step, and that the equations are established in the space-fixed coordinate system in order to make their method more adaptive. The free-surface condition is still linear, so that the time-domain Green function can be used.

In de Kat's work (1990), the Froude-Krylov forces were calculated with the instantaneous wetted hull surface. The work done by de Kat et al. (1994) has led to the development of safety criteria for ships operating in severe seas. In this work, linearized radiation and diffraction forces are assumed for the simulation of ship motion in waves. However, other forces, such as the Froude-Krylov force, viscous damping force, and maneuvering forces, are nonlinear. This approach might be less rigorous, but it was used in the capsize analysis (Huang et al., 1998), and provides satisfactory results.

It is almost impossible to directly solve the boundary-value problem of the radiation and diffraction potentials for a long-time simulation on a personal computer, because the computation of memory effects of wave and motion is very time-consuming. The impulse function method given by Cummins (1962) introduced an effective way to solve this cumbersome problem. Beck and King (1989) use the Fourier transform to obtain the impulse response

functions of the radiated wave forces. However, the Fourier transform has to be cut off at a certain frequency to achieve convergent results. This method is not readily amenable to practical applications, because an appropriate cut-off frequency needs to be determined by numerical experiment for individual ships. In this work, the discretized Fredholm integral equation of the first kind for the response function is solved directly in the time domain at each instant. This method was found to be robust without much numerical difficulty.

2 Nonlinear Ship Motion in the Time Domain

Three coordinate systems are employed for the ship motion analysis as shown in Fig. 1.

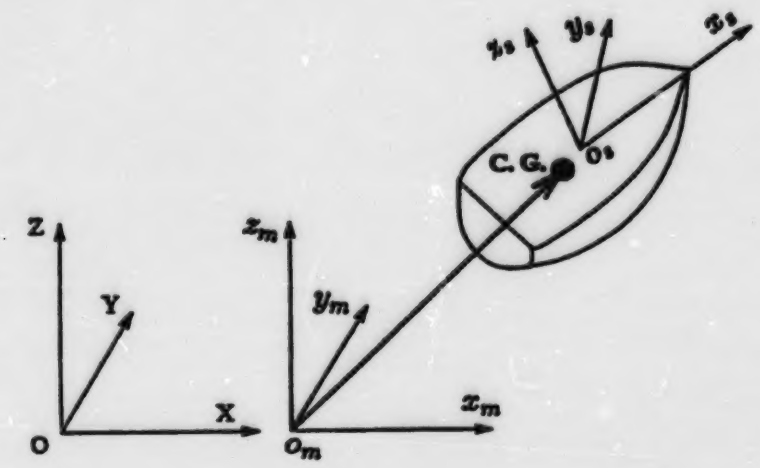

Figure 1: Coordinate Systems for Ship Motions

Here, $OXYZ$ is the space-fixed coordinate system with the OXY plane on the calm water surface and the OZ axis is positive upwards. The second coordinate system $o_m x_m y_m z_m$ is a moving system which moves at the steady forward speed of the ship, U, in the OX direction. At $t = 0$, o_m coincides with O. The $o_m x_m y_m$ plane always coincides with the OXY plane. The $o_m x_m$ axis is in the same direction as the OX axis, and the $o_m z_m$ axis is positive upwards. The third coordinate system $o_s x_s y_s z_s$ is fixed on the ship. The origin o_s coincides with o_m and the $o_s x_s y_s$ plane is coincided with the OXY plane when the ship is at its static equilibrium position, and the $o_s z_s$ axis is positive upwards.

2.1 Equations of Ship Motion

The oscillatory ship motions are described in the $o_m x_m y_m z_m$ system. The ship motions are represented by $(\xi_1, \xi_2, \xi_3, e_1, e_2, e_3)$, in which, (ξ_1, ξ_2, ξ_3) are the displacements of the

centre of gravity, and (e_1, e_2, e_3) are the Eulerian angles between the $o_s x_s y_s z_s$ frame and the $o_m x_m y_m z_m$ frame. The Eulerian angles are the measurements of the ship's rotation about the axes which pass through the centre of gravity of the ship. The instantaneous translational velocities of ship motion in the directions of $o_s x_s$, $o_s y_s$ and $o_s z_s$ are denoted by u_1, u_2 and u_3, respectively, and the angular velocities about axes parallel to $o_s x_s$, $o_s y_s$ and $o_s z_s$ passing through the centre of gravity u_4, u_5 and u_6, respectively. The equations of ship motion are:

$$[m_{kj}] \begin{pmatrix} \dot{u}_1 \\ \dot{u}_2 \\ \dot{u}_3 \\ \dot{u}_4 \\ \dot{u}_5 \\ \dot{u}_6 \end{pmatrix} + \begin{pmatrix} m\vec{\Omega} \times \vec{u} \\ \\ \vec{\Omega} \times ([I]\vec{\Omega}) \end{pmatrix} = \begin{pmatrix} F_1 \\ F_2 \\ F_3 \\ F_4 \\ F_5 \\ F_6 \end{pmatrix} \tag{1}$$

where $\vec{u} = (u_1, u_2, u_3)$, $\vec{\Omega} = (u_4, u_5, u_6)$, $[m_{kj}]$ is the generalized mass matrix:

$$[m_{kj}] = \begin{bmatrix} m & 0 & 0 & 0 & 0 & 0 \\ 0 & m & 0 & 0 & 0 & 0 \\ 0 & 0 & m & 0 & 0 & 0 \\ 0 & 0 & 0 & I_{11} & 0 & -I_{13} \\ 0 & 0 & 0 & 0 & I_{22} & 0 \\ 0 & 0 & 0 & -I_{13} & 0 & I_{33} \end{bmatrix} \tag{2}$$

and $[I]$ is the moment of inertia matrix

$$[I] = \begin{bmatrix} I_{11} & 0 & -I_{13} \\ 0 & I_{22} & 0 \\ -I_{13} & 0 & I_{33} \end{bmatrix} \tag{3}$$

in which m is the mass of the ship, I_{kk} $(k = 1, 2, 3)$ denote the moments of inertia of the ship, and I_{kj} $(k \neq j)$ are the products of inertia of the ship. The total external forces on the ship are

$$\begin{aligned} F_k(t) \;=\; & F_k^{Rs}(t) + F_k^{FK}(t) + F_k^{Dif}(t) + F_k^{Rad}(t) \\ & + F_k^{\nu}(t) + F_k^{Prop}(t) + F_k^{H}(t) + F_k^{Rud}(t) \\ & \text{for } k = 1, 2, \cdots, 6 \end{aligned} \tag{4}$$

where F_k^{Rs} are the restoring forces; F_k^{FK} nonlinear Froude-Krylov forces; F_k^{Dif} the diffracted wave forces; F_k^{Rad} the radiated wave forces; F_k^{ν} the viscous forces including viscous roll damping moment, resistance and cross-flow drag; F_k^{Prop} the propeller thrust; F_k^{H} the hull maneuvering forces; and F_k^{Rud} the rudder force.

Brief descriptions of the methods of computing F_k^{Rs}, F_k^{FK}, F_k^{ν}, F_k^{Prop}, F_k^{H}, and F_k^{Rud} are given below in this chapter. The radiated wave forces and diffracted wave forces computed

by the time-domain Green function are given in chapter 3. Details of the computation of the force components may be found in Huang (1995).

The ship translational displacements (ξ_1, ξ_2, ξ_3) in the steady moving system and the Eulerian angles (e_1, e_2, e_3) are solved from:

$$\begin{pmatrix} \dot{\xi}_1 \\ \dot{\xi}_2 \\ \dot{\xi}_3 \\ \dot{e}_1 \\ \dot{e}_2 \\ \dot{e}_3 \end{pmatrix} = \begin{bmatrix} [R] & 0 \\ 0 & [B] \end{bmatrix} \begin{pmatrix} u_1 \\ u_2 \\ u_3 \\ u_4 \\ u_5 \\ u_6 \end{pmatrix} \tag{5}$$

where matrices $[B]$ and $[R]$ are defined as follows:

$$[B] = \begin{bmatrix} 1 & s_1 t_2 & c_1 t_2 \\ 0 & c_1 & -s_1 \\ 0 & s_1/c_2 & c_1/c_2 \end{bmatrix} \tag{6}$$

$$[R] = \begin{pmatrix} c_2 c_3 & s_1 s_2 c_3 - c_1 s_3 & c_1 s_2 c_3 + s_1 s_2 \\ c_2 s_3 & s_1 s_2 s_3 + c_1 c_3 & s_1 s_2 s_3 - s_1 c_3 \\ -s_2 & s_1 c_2 & c_1 c_2 \end{pmatrix} \tag{7}$$

and $c_i = \cos e_i$, $s_i = \sin e_i$, and $t_i = \tan e_i$ for $i = 1, 2, 3$.

The ship motions in the time domain are solved simultaneously from twelve equations in both (1) and (5). At each time step, the motion velocities in the ship-fixed coordinate system are obtained by integrating the accelerations, which are the solution of (1), with the velocities at the previous time step as the initial conditions. The ship motion displacements are found by integrating the motion velocities in the steady moving coordinate system, which are the solution of (5). The ship motion at a new time step, which is unknown, is required to compute the forces (e.g. the restoring force has to be calculated with the ship motion displacement), and the linear prediction based on stochastic theory is adopted to determine the ship motion for the force computation. With the predicted ship motion at $t = t_{n+1}$, the external forces are evaluated. Then, the ship motion is solved numerically from the first order ordinary differential equations (1) and (5) by the Extrapolation Method (Magee, 1994; Huang, 1995).

2.2 Nonlinear Froude-Krylov Forces

At each time instant, the ship motions $(\xi_1, \xi_2, \xi_3, e_1, e_2, e_3)$ are solved from equations (1) and (5). Making use of the Eulerian angles (e_1, e_2, e_3), the ship-fixed coordinate system and the

steady moving coordinate system can be related as:

$$\begin{pmatrix} x_m \\ y_m \\ z_m \end{pmatrix} = \begin{pmatrix} \xi_1 + x_{sg} \\ \xi_2 + y_{sg} \\ \xi_3 + z_{sg} \end{pmatrix} + [R] \begin{pmatrix} x_s - x_{sg} \\ y_s - y_{sg} \\ z_s - z_{sg} \end{pmatrix} \tag{8}$$

where (x_{sg}, y_{sg}, z_{sg}) are the coordinates of the centre of gravity of the ship in the ship-fixed coordinate system. Also, we have

$$X = Ut + x_m, \quad Y = y_m \quad \text{and} \quad Z = z_m \tag{9}$$

where U is the forward speed of the ship.

In computer simulation, the wave profile $\zeta_0(X, Y, t)$ is first computed, and then all the nodal points on the ship hull and deck are transformed into the $OXYZ$ coordinate system using equations (8) and (9). If a nodal point is below the free surface $\zeta_0(X, Y, t)$, then we compute the pressure at this point:

$$P(X, Y, Z, t) = P_s(X, Y, Z, t) + P_d(X, Y, Z, t) \tag{10}$$

where, the static pressure is:

$$P_s(X, Y, Z, t) = -\rho g[Z - \zeta_0(X, Y, t)] \tag{11}$$

and the dynamic pressure is:

$$P_d(X, Y, Z, t) = -\rho \frac{\partial \Phi_0}{\partial t} - \frac{1}{2}\rho |\nabla \Phi_0|^2 \tag{12}$$

In this work, quadrilateral panels are used to discretize the ship hull surface. It is assumed that at the instant t_n, there are $N(t_n)$ wetted panels on the hull surface and the deck space. The mean pressure on a panel is:

$$\bar{P} = \frac{1}{4} \sum_{i=1}^{4} p_i(X, Y, Z, t) \tag{13}$$

where p_i is the pressure at a nodal point of the panel. The nonlinear restoring forces are computed as follows:

$$F_k^{Rs}(t) = -\sum_{j=1}^{N(t_n)} \bar{P}_{s,j} \Delta S_j n_{k,j} \quad k = 1, 2, \cdots, 6 \tag{14}$$

where ΔS_j is the area of the j^{th} panel and $n_{k,j}$ is the k^{th} component of the unit normal on the j^{th} panel. The nonlinear Froude-Krylov forces are:

$$F_k^{FK}(t_n) = -\sum_{j=1}^{N(t_n)} \bar{P}_{d,j} \Delta S_j n_{k,j} \quad k = 1, 2, \cdots, 6 \tag{15}$$

where the subscript "d" indicates the dynamic pressure.

2.3 Viscous Forces and Moments

2.3.1 Viscous Roll Damping

For large-amplitude ship motions, the linear-plus-quadratic model is used:

$$F_4^v(\dot{e}_1) = (\alpha_1^v + \alpha_2^v|\dot{e}_1|)\dot{e}_1 \tag{16}$$

where α_1^v and α_2^v are the linear-quadratic viscous roll damping coefficients, which can be determined either by model tests or by empirical formulae.

In case no appropriate test data are available, one option is to use Schmitke's (1978) empirical formulae for frigates. However, all existing empirical formulae are expressed in the frequency-domain as functions of roll amplitude and frequency. In (16) we need to express the roll damping as a function of the instantaneous roll velocity. A method converting the frequency-domain roll damping into the time-domain is given by Huang and Hsiung (1997), which is briefly described as follows.

Figures 13 and 14 are body plan and the panelized hull surface, respectively, for Series 60 Block 70. Roll damping was computed for this hull in the frequency domain. Figure 15 shows the roll damping coefficients against frequency at $F_n = 0.2$ with various roll amplitudes. Multiplying the roll amplitude and frequency gives the roll velocity. From this family of curves in Fig.15, it can be found that at the same roll velocity, the roll damping coefficients are the same regardless of the amplitude and frequency of roll. This indicates that the damping coefficients depend on roll velocity only. Therefore, we fit the damping coefficient by a quadratic polynomial, and the coefficients of the polynomial are the coefficients of the roll damping α_1^v and α_2^v. The fitted damping curve for Series 60 Block 70 hull is shown in Fig.16. It can be seen that the fitted curve is very close to the one predicted by Schmitke's formula. A similar approach may be used to estimate α_1^v and α_2^v for other hull forms.

2.3.2 Resistance

The resistance and the cross-flow drag are important to surge, sway and yaw in the time-domain simulation. It is recommended that the resistance model test data for the hull under consideration be used in the computation. If there is no test data available, empirical formulae, such as those given by Holtrop and Mennen (1982), should be used for resistance estimation.

2.3.3 Cross-Flow Drag

The cross-flow drag and moment are calculated by:

$$F_2^v(t) = -\frac{1}{2}\rho \int_L C_d(x_s)T(x_s)v_2(x_s,t)|v_2(x_s,t)|dx_s \tag{17}$$

and

$$F_6^v(t) = -\frac{1}{2}\rho \int_L x_s C_d(x_s)T(x_s)v_2(x_s,t)|v_2(x_s,t)|dx_s \tag{18}$$

where $C_d(x_s)$ is the sectional cross-flow drag coefficient, $T(x_s)$ is the local draft of the ship, L is the ship length, and $v_2(x_s,t)$ is the transverse relative velocity between the hull and the water particle of the local cross-flow.

2.4 Propeller Thrust

The thrust and torque of the propeller can be determined by propeller charts as a function of J:

$$F_1^{Prop} = (1-t_p)\rho n_p^2 D_p^4 K_T(J) \tag{19}$$

and

$$F_4^{Prop} = \rho n_p^2 D_p^5 K_Q(J) \tag{20}$$

where J is the advancing coefficient, t_p the thrust deduction fraction, n_p the revolution per second, D_p the propeller diameter, J the advancing coefficient, K_T the thrust coefficient, and K_Q the torque coefficient. The coefficients t_p, J, K_T, and K_Q can be estimated from available propeller charts.

2.5 Maneuvering Forces

The following nonlinear lateral force and turning moment are adopted in the seakeeping computation (Kijima et al., 1990):

$$\begin{aligned} F_2^H(t) = &\frac{1}{2}\rho L d\tilde{U}^2(Y_\beta\beta' + Y_r r' + Y_{\beta\beta}|\beta'|\beta' \\ &+Y_{rr}|r'|r' + (Y_{\beta\beta r}\beta' + Y_{\beta rr})\beta' r' \end{aligned} \tag{21}$$

and

$$\begin{aligned} F_6^H(t) = &\frac{1}{2}\rho L^2 d\tilde{U}^2(N_\beta\beta' + N_r r' + N_{\beta\beta}|\beta'|\beta' \\ &+N_{rr}|r'|r' + (N_{\beta\beta r}\beta' + N_{\beta rr})\beta' r' \end{aligned} \tag{22}$$

where L is ship length, d is ship draft, $\beta' = -u_2/\tilde{U}$ and $r' = \dot{e}_6 L/\tilde{U}$. In the computation, $\tilde{U}$ is the instantaneous forward speed (the ship's mean forward speed plus the surge velocity), and u_2 the instantaneous sway velocity. The hydrodynamic derivatives $Y's$ and $N's$ are determined by empirical formulae or from test results.

2.6 Rudder Forces and Autopilot

The rudder angle δ is defined as being positive when it is turned to the port side. From the paper by Kijima et al. (1990), the normal force acting on the rudder can be evaluated by:

$$F_N = -\frac{1}{2}\rho \frac{6.13\tilde{\lambda}}{\tilde{\lambda}+2.25} A_r V_r^2 \sin\delta_e \tag{23}$$

where $\tilde{\lambda}$ is the aspect ratio of the rudder, A_r the rudder area of a single side, V_r the relative velocity of the water particle to the rudder, and δ_e the effective rudder angle:

$$\delta_e = \delta + \tan^{-1}\frac{u_2 - l_z\dot{e}_6 + l_x\dot{e}_4}{\bar{U}+u_1} \tag{24}$$

Suppose that the normal force acts on the pressure point C_{rud} on the rudder, the rudder force components can be obtained as follows:

$$F_1^{Rud} = -|F_N|\sin\delta \tag{25}$$

$$F_2^{Rud} = F_N\cos\delta \tag{26}$$

$$F_4^{Rud} = l_z F_N\cos\delta \tag{27}$$

and

$$F_6^{Rud} = -l_x F_N\cos\delta \tag{28}$$

where l_x and l_z are horizontal and vertical distances between the pressure point C_{rud} and the centre of gravity, respectively; U_{cx} and U_{cy} are the longitudinal and lateral components of current, respectively.

The following autopilot is considered for course keeping purposes:

$$\delta(t) = \begin{cases} \alpha_1^r e_6(t) + \alpha_2^r \dot{e}_6, & \text{if } e_6 > \delta_0 \\ 0, & \text{if } e_6 \le \delta_0 \end{cases} \tag{29}$$

where α_1^r is the yaw gain, α_2^r is the yaw rate gain, and δ_0 is the threshold value of yaw beyond which the rudder is activated.

3 Forces due to the Radiated and Diffracted Waves

3.1 Solutions of the Radiated Wave Potentials

Generally speaking, the radiation and diffraction potentials in equations (125) through (130) in Appendix A can be solved to simulate the ship motions. But it is almost impossible directly to solve this boundary-value problem for a long-time simulation on a personal computer, because the computation of memory effects of wave and motion, that is, computing the convolution product of the time-domain Green function, is very time-consuming. Alternatively, the impulse response function method is used to describe the radiation forces on the ship hull. This method was originally introduced by Cummins (1962) to discuss the radiation problem and to relate the time-domain hydrodynamic forces to the hydrodynamic forces of the frequency domain. The radiation potential is caused not only by the oscillatory velocity but also by the oscillatory displacement, which changes the position of the body in the steady flow field. The ship motion changes the distribution of the gradient of the steady flow velocity on the body surface. The corresponding fluid motion can be separated into two parts: the impulsive motion and the subsequent wave motion.

During the impulsive motion, the ship is given an impulsive displacement η_j which can be considered to consist of a movement at the velocity $\dot{\eta}_j$ for a very small time interval Δt, and then the ship motion is terminated abruptly at the end of the time interval,

$$\eta_j = \dot{\eta}_j \Delta t \tag{30}$$

Hence, the velocity potential, which is referred as the impulsive potential, can be expressed as:

$$\dot{\eta}_j \psi_j(P) + \eta_j \chi_j(P)$$

From Appendix A, ψ_j satisfies the following conditions:

$$\nabla^2 \psi_j = 0 \tag{31}$$

$$\psi_j = 0, \quad \text{on} \quad z_m = 0 \tag{32}$$

$$\frac{\partial \psi_j}{\partial n} = n_j \quad \text{on} \quad \bar{S}, \tag{33}$$

$$\nabla \psi_j \to 0 \quad \text{as} \quad R \to \infty \quad \text{on} \quad z_m = 0, \tag{34}$$

and

$$\nabla \psi_j \to 0 \quad \text{as} \quad z_m \to -\infty. \tag{35}$$

The function, χ_j, which is due to the displacement of ship motion in the steady flow field, satisfies the following conditions:

$$\nabla^2 \chi_j = 0 \tag{36}$$

$$\chi_j = 0, \quad \text{on} \quad z_m = 0 \tag{37}$$

$$\frac{\partial \chi_j}{\partial n} = m_j \quad \text{on} \quad \bar{S}, \tag{38}$$

$$\nabla \chi_j \to 0 \quad \text{as} \quad R \to \infty \quad \text{on} \quad z_m = 0, \tag{39}$$

and

$$\nabla \chi_j \to 0 \quad \text{as} \quad z_m \to -\infty, \tag{40}$$

where m_j is the so-called m-terms (see equations(138) and (139) below), $\bar{S}$ is the mean wetted surface of the ship hull, and $R = \sqrt{x_m^2 + y_m^2}$.

During the impulsive phase, the free surface is elevated by an amount

$$\Delta\zeta_j = (\dot{\eta}_j \frac{\partial \psi_j}{\partial z_m} + \eta_j \frac{\partial \chi_j}{\partial z_m})\Delta t \tag{41}$$

After the impulse, this elevation will disperse and consequently cause motion of the fluid. The corresponding velocity potential, which is referred to as the wave potential, is proportional to the motion of the ship, i.e.

$$\Psi_j(P,t) = \eta_j \varphi_j(P,t) = \dot{\eta}_j \varphi_j(P,t)\Delta t \tag{42}$$

φ_j satisfies the following conditions:

$$\nabla^2 \varphi_j(P,t) = 0 \tag{43}$$

$$(\frac{\partial}{\partial t} - U\frac{\partial}{\partial x_m})^2(\varphi_j + \chi_j) = 0 \quad \text{on} \quad z_m = 0 \quad \text{for} \quad t \geq 0, \tag{44}$$

$$\frac{\partial \varphi_j}{\partial n} = 0 \quad \text{on} \quad \bar{S} \quad \text{for} \quad t \geq 0 \tag{45}$$

$$\frac{\partial \varphi_j}{\partial t} = -g\frac{\partial \psi_j}{\partial z_m} \quad \text{on} \quad z_m = 0 \quad \text{for} \quad t = 0 \tag{46}$$

$$\frac{\partial^2 \varphi_j}{\partial t^2} = -g\frac{\partial \chi_j}{\partial z_m} \quad \text{on} \quad z_m = 0 \quad \text{for} \quad t = 0 \tag{47}$$

$$\nabla \varphi_j \to 0 \quad \text{as} \quad R \to \infty \quad \text{on} \quad z_m = 0, \tag{48}$$

and

$$\nabla \varphi_j \to 0 \quad \text{as} \quad z_m \to -\infty. \tag{49}$$

If the ship undergoes a small-amplitude motion $\eta_j(t)$ in the j^{th} mode, the potential of the radiated waves will be:

$$\phi_j(P,t) = \dot{\eta}_j(t)\psi_j(P) + \eta_j(t)\chi_j(P) + \int_{-\infty}^{t} \varphi_j(P, t-\tau)\dot{\eta}_j(\tau)d\tau. \tag{50}$$

It can be shown that $\phi_j(P,t)$ satisfies the free surface condition, the body surface boundary condition, and the far-field condition.

The functions χ_j, ψ_j and the potential ϕ_j can be expressed using different source strength distributions:

$$\chi_j(P) = -\frac{1}{4\pi}\int\int_S \sigma_j^{\chi}(Q)(\frac{1}{r}-\frac{1}{r_1})dS \tag{51}$$

$$\psi_j(P) = -\frac{1}{4\pi}\int\int_S \sigma_j^{\psi}(Q)(\frac{1}{r}-\frac{1}{r_1})dS \tag{52}$$

$$\begin{aligned}\phi_j(P,t) &= -\frac{1}{4\pi}\int_0^t d\tau \int\int_S \sigma_j(Q,\tau)G(P,Q,t-\tau)dS \\ &\quad -\frac{U^2}{4\pi g}\int_0^t d\tau \oint_\Gamma n_1\sigma_j(Q,\tau)G(P,Q,t-\tau)d\eta\end{aligned} \tag{53}$$

where G is the time-domain Green function as defined in Appendix B and Γ is the contour of the mean waterline. The method to compute the Green function used in this work was given by Huang and Hsiung (1991).

Using the boundary condition on the body surface, the values of the source strength can be determined from the following integral equation:

$$-\frac{\sigma_j^{\chi}(P)}{2} - \frac{1}{4\pi}\int\int_S \sigma_j^{\chi}(Q)\frac{\partial}{\partial n_P}(\frac{1}{r}-\frac{1}{r_1})dS = n_j(P) \tag{54}$$

$$-\frac{\sigma_j^{\psi}(P)}{2} - \frac{1}{4\pi}\int\int_S \sigma_j^{\psi}(Q)\frac{\partial}{\partial n_P}(\frac{1}{r}-\frac{1}{r_1})dS = m_j(P) \tag{55}$$

$$\begin{aligned}\frac{\partial\phi_j(P,t)}{\partial n_P} &= -\frac{\sigma_j(P,t)}{2} - \frac{1}{4\pi}\int_0^t d\tau \int\int_S \sigma_j(Q,\tau)\frac{\partial G(P,Q,t-\tau)}{\partial n_P}dS \\ &\quad -\frac{U^2}{4\pi g}\int_0^t d\tau \oint_\Gamma n_1\sigma_j(Q,\tau)\frac{\partial G(P,Q,t-\tau)}{\partial n_P}d\eta\end{aligned} \tag{56}$$

The numerical scheme for the solution of (56) is given in Appendix C.

3.2 Forces due to the Radiated Waves

According to the Cauchy-Lagrange integral in a steady moving coordinate system, the hydrodynamic pressure can be determined by

$$p_j(P,t) = -\rho\frac{\partial(\bar{\Phi}(P)+\phi_j(P,t))}{\partial t} - U\frac{\partial(\bar{\Phi}(P)+\phi_j(P,t))}{\partial x_m} - \frac{1}{2}\rho|\nabla(\bar{\Phi}(P)+\phi_j(P,t))|^2. \tag{57}$$

where $\bar{\Phi}$ is the steady wave potential function.

The linearized unsteady part of the pressure is

$$p_j = -\rho\frac{\partial\phi_j}{\partial t} - \rho\vec{\bar{W}}\cdot\nabla\phi_j \tag{58}$$

where $\vec{\bar{W}} = \nabla\bar{\Phi}$.

Then, the hydrodynamic forces can be obtained by integrating the pressure over the wetted hull surface:

$$F_{kj}(t) = \int\int_S pn_k dS = -\rho\int\int_S \frac{\partial\phi_j}{\partial t}n_k dS - \rho\int\int_S(\vec{\bar{W}}\cdot\nabla\phi_j)n_k dS \tag{59}$$

According to the relation presented in the paper by Ogilvie and Tuck (1969):

$$\int\int_S[m_k\phi_j + n_k(\vec{\bar{W}}\cdot\nabla\phi_j)]dS = -\oint_\Gamma n_k\phi_j(\vec{l}\times\vec{n})\cdot\vec{\bar{W}}dl, \tag{60}$$

the unsteady hydrodynamic force is obtained:

$$F_{kj}(t) = -\rho\int\int_S\frac{\partial\phi_j}{\partial t}n_k dS + \rho\int\int_S\phi_j m_k dS + \rho\oint_\Gamma n_k\phi_j(\vec{l}\times\vec{n})\cdot\vec{\bar{W}}dl. \tag{61}$$

Substituting (50) into (61), we have:

$$F_{kj}(t) = -\bar{\mu}_{kj}\ddot{\eta}_j(t) - \bar{\lambda}_{kj}\dot{\eta}_j(t) - \bar{\gamma}_{kj}\eta_j(t) - \int_0^t K_{kj}(t-\tau)\dot{\eta}_j(\tau)d\tau \tag{62}$$

where

$$\bar{\mu}_{kj} = \rho\int\int_S\psi_j n_k dS \tag{63}$$

is the time-domain added mass of the ship,

$$\bar{\lambda}_{kj} = \rho[\int\int_S\chi_j n_k dS - \int\int_S\psi_j m_k dS - \oint_\Gamma\psi_j m_k(\vec{l}\times\vec{n})\cdot\vec{\bar{W}}dl], \tag{64}$$

is the time-domain hydrodynamic damping,

$$\bar{\gamma}_{kj} = \rho[-\int\int_S\chi_j m_k dS - \oint_\Gamma\chi_j n_k(\vec{l}\times\vec{n})\cdot\vec{\bar{W}}dl] \tag{65}$$

is the coefficient of the time-domain hydrodynamic restoring force, and

$$\begin{aligned} K_{kj}(t) \;=\; & \rho[\int\int_S\frac{\partial\varphi_j(Q,t)}{\partial t}n_k dS - \int\int_S\varphi_j(Q,t)m_k dS \\ & - \oint_\Gamma n_k\varphi_j(Q,t)(\vec{l}\times\vec{n})\cdot\vec{\bar{W}}dl] \end{aligned} \tag{66}$$

is the memory function. The total radiation force is obtained from:

$$F_k^{Rad}(t) = \sum_{j=1}^{6}F_{kj}(t) \tag{67}$$

In SEALOADS program, the responses of the radiation force and the diffraction force to the input have been linearized. Hence, all the methods describing a linear system response can be applied. The approach in SEALOADS is to obtain the impulse response functions by introducing a non-impulse input instead of solving equation (56) in the whole time duration of motion simulation. When we solve the motion equation, we choose the radiation force expressed by (62). The radiation force in (59) can be transformed into the form of (62) by employing the following non-impulse motion:

$$\dot{\eta}_j(t) = \sqrt{\frac{\bar{a}L}{\pi g}} e^{-\bar{a}t^2} \tag{68}$$

where $\bar{a}$ is an arbitrary constant to be specified and L is the ship length.

The boundary condition on the body surface will be

$$\frac{\partial \phi_j(P,t)}{\partial n_p} = \sqrt{\frac{\bar{a}L}{\pi g}} e^{-\bar{a}t^2} n_j + \frac{1}{2}\sqrt{\frac{L}{g}}[1 + \mathrm{erf}(\sqrt{\bar{a}}t)]m_j. \tag{69}$$

After substituting (69) into (56), the time history of the source strength can be found. Since the non-impulse motion decays very fast, the computation for the radiated waves will be quite efficient. Then, the potential functions and the radiation forces can be determined from (53) and (59), respectively.

Let the radiation force (61) be expressed as:

$$F_{ij}(t) = -\dot{g}_{ij}(t) - h_{ij}(t), \tag{70}$$

where

$$g_{ij}(t) = \rho \int\int_S \phi_j n_i dS, \tag{71}$$

$$h_{ij}(t) = -\rho \int\int_S \phi_j m_i dS - \rho \oint_\Gamma \phi_j (\vec{l} \times \vec{n}) \cdot \vec{W} n_i d\eta. \tag{72}$$

Equating (70) and (62), we have

$$\int_0^t K_{ij}(t-\tau)\dot{\eta}_j(\tau)d\tau = \dot{g}_{ij}(t) + h_{ij}(t) - \mu_{ij}\ddot{\eta}_j(t) - \lambda_{ij}\dot{\eta}_j(t) - \gamma_{ij}\eta_j(t). \tag{73}$$

The kernel function K_{ij} can be obtained by solving the Fredholm integral equation of the first kind. It can be seen that the values of $\partial\phi_j/\partial t$ and $\nabla\phi_j$ are not required in computing the radiation forces, so that much computational work can be saved.

Beck and King (1989) applied the Fourier transform to determine the response functions K_{ij}. The difficulty with their method is that the inverse Fourier transform has to be cut off at a certain frequency to reach convergent results. The desirable cut-off frequency for a given mode varies for different hull forms and forward speeds, and can only be determined by numerical experiment.

In the present method, K_{ij} is determined by solving the integral equation (73) directly in the time domain; that is, by solving the following systems of linear equations at each time step:

$$\sum_{n=1}^{m-1}(K_{ij})_{m-n}(\eta_j)_n + \frac{1}{2}[(K_{ij})_m(\eta_j)_0 + (K_{ij})_0(\eta_j)_m] = \frac{(f_{ij})_m}{\Delta t} \tag{74}$$

where $m = 1, 2, ..., M$, M is the total number of time steps defined by $T = M\Delta t$, and T is the upper limit of the integration in equation (73). Because (74) is a system of M equations in $M+1$ unknown, an additional equation is needed to make the solution unique. The choice of possible additional constraint is explained in Section 5.2 below.

The method has been tested for several floating bodies with different body shapes. Some results are presented below. Fig.2 shows the panelized surface of a hemi-sphere. Fig.3 shows the computed response function $K_{33}(t)$ for a hemi-sphere of radius $R = 5$ m compared with Barakat's result (1962). By using the response function $K_{33}(t)$ and the Fourier transformation, the corresponding added mass and damping coefficients in the frequency domain can be found (Liapis and Beck, 1985). Fig.4 shows the comparison of the present results with Barakat's results. Similarly, for the panelized surface for the Series 60 ($C_B = 0.7$) hull shown in Fig.5 , the function $K_{33}(t)$ is calculated and compared with Liapis' results in Fig.6. Comparisons of added mass and damping coefficients are shown in Fig.7.

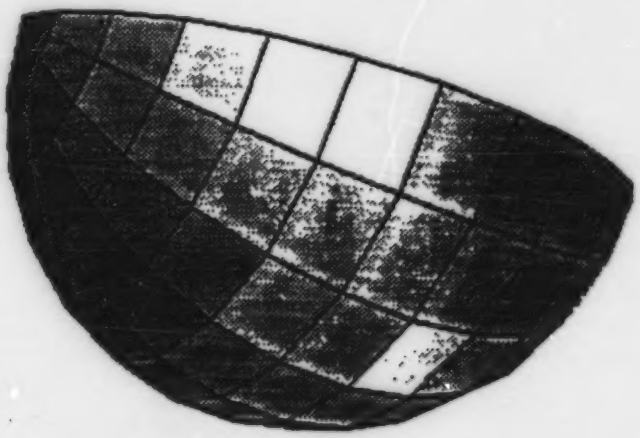

Figure 2: Panelization of a Hemi-sphere

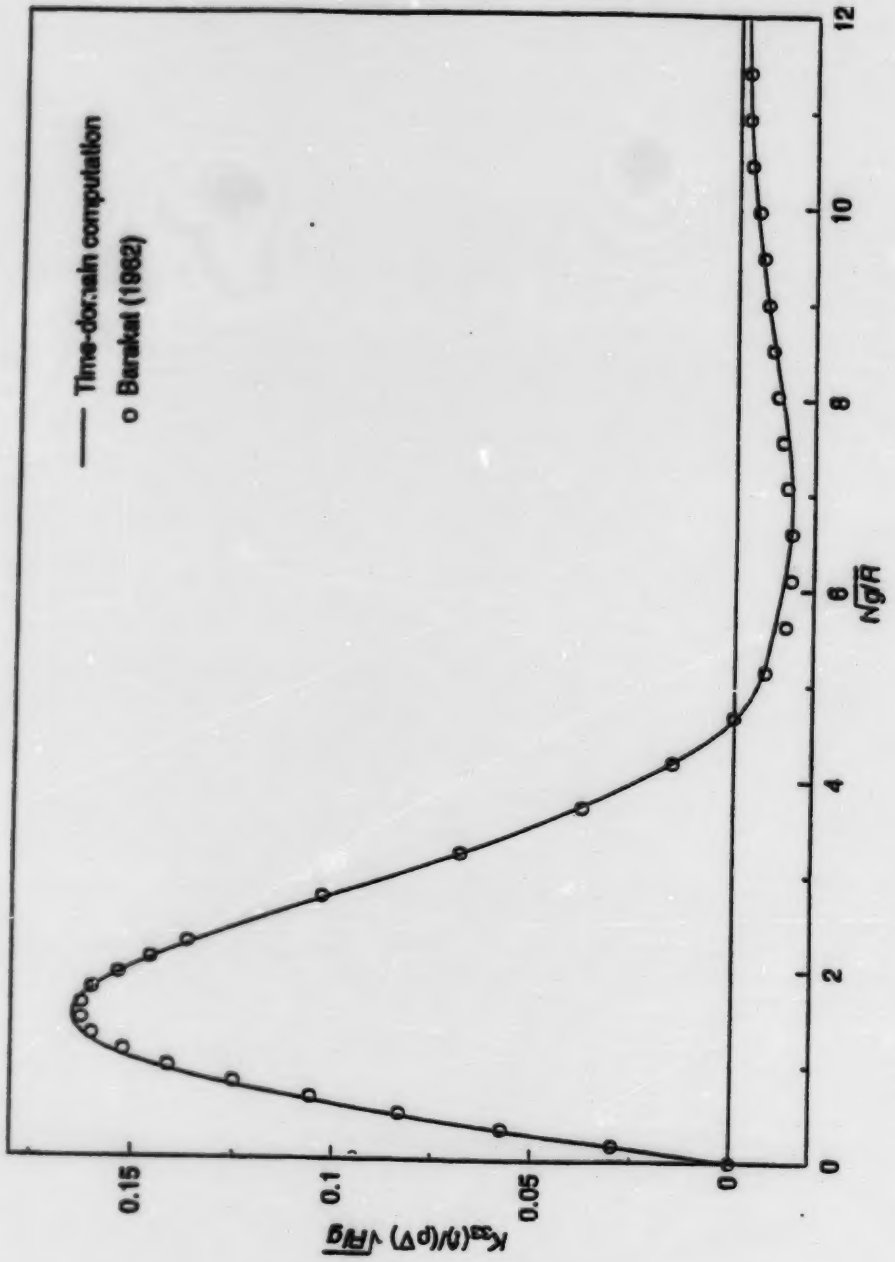

Figure 3: Response function $K_{33}(t)$ of a hemisphere ($F_n = 0$)

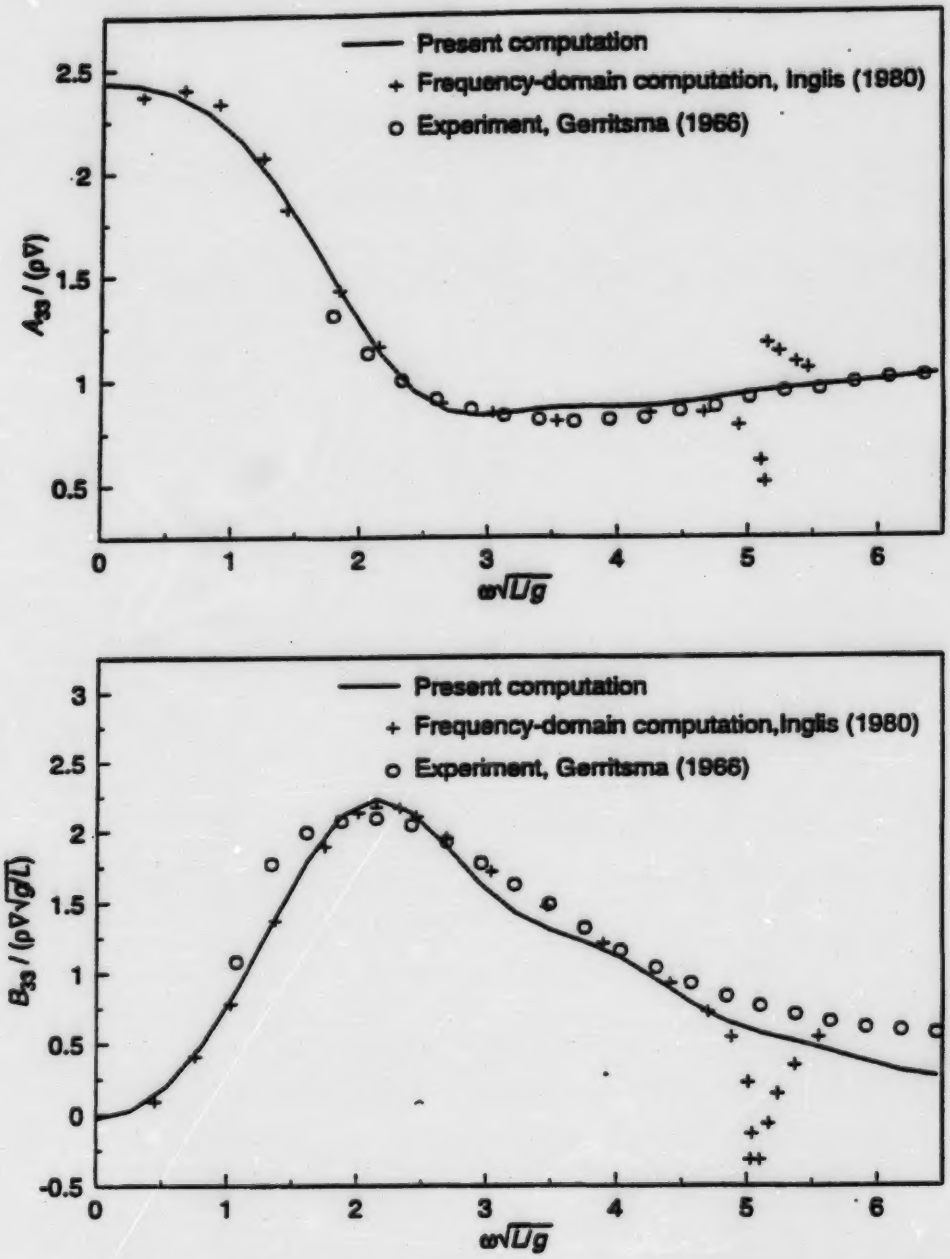

Figure 4: Added mass and damping coefficient of a hemisphere ($F_n = 0$)

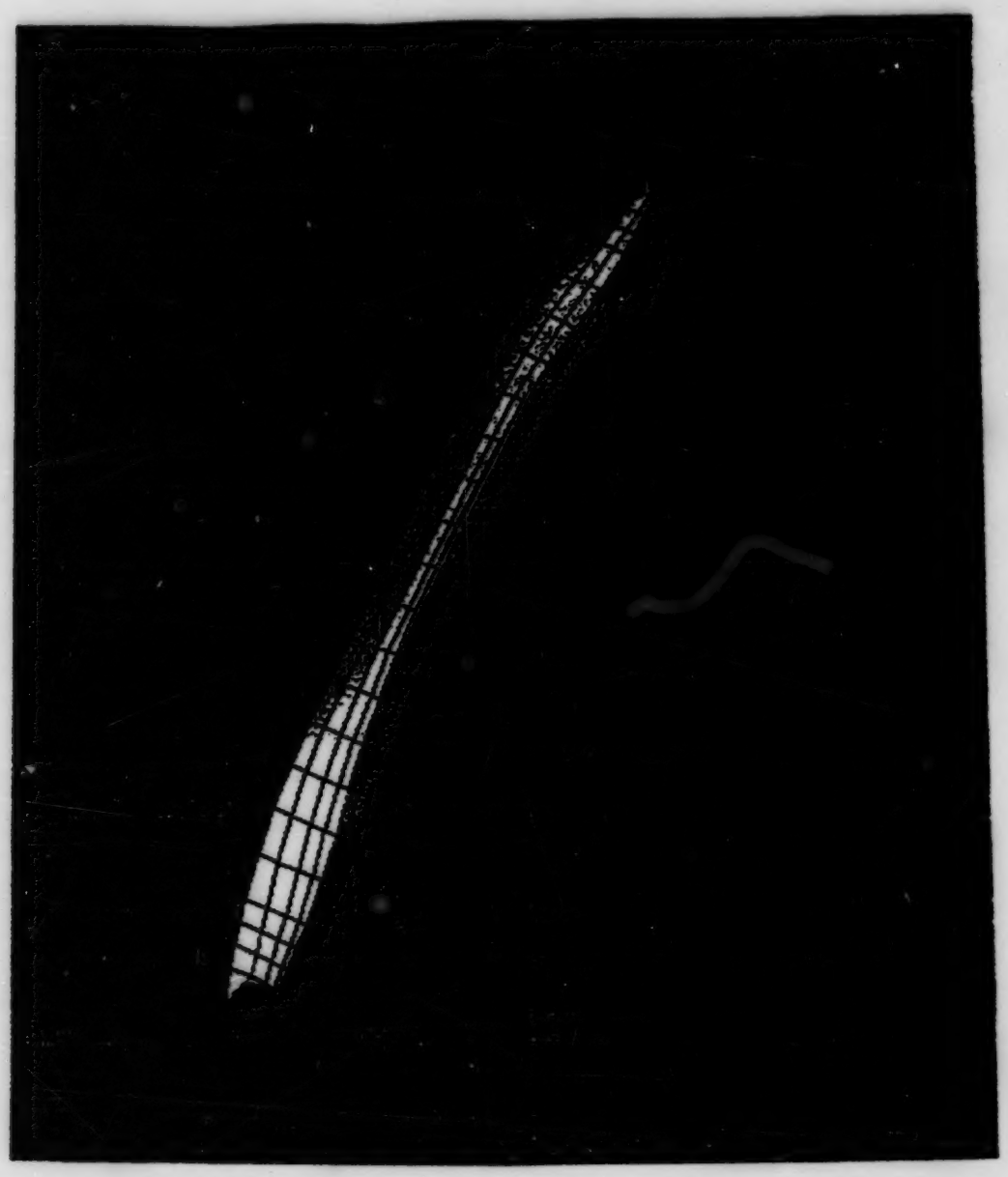

Figure 5: Panelization of a Series 60 (C_B=0.7)

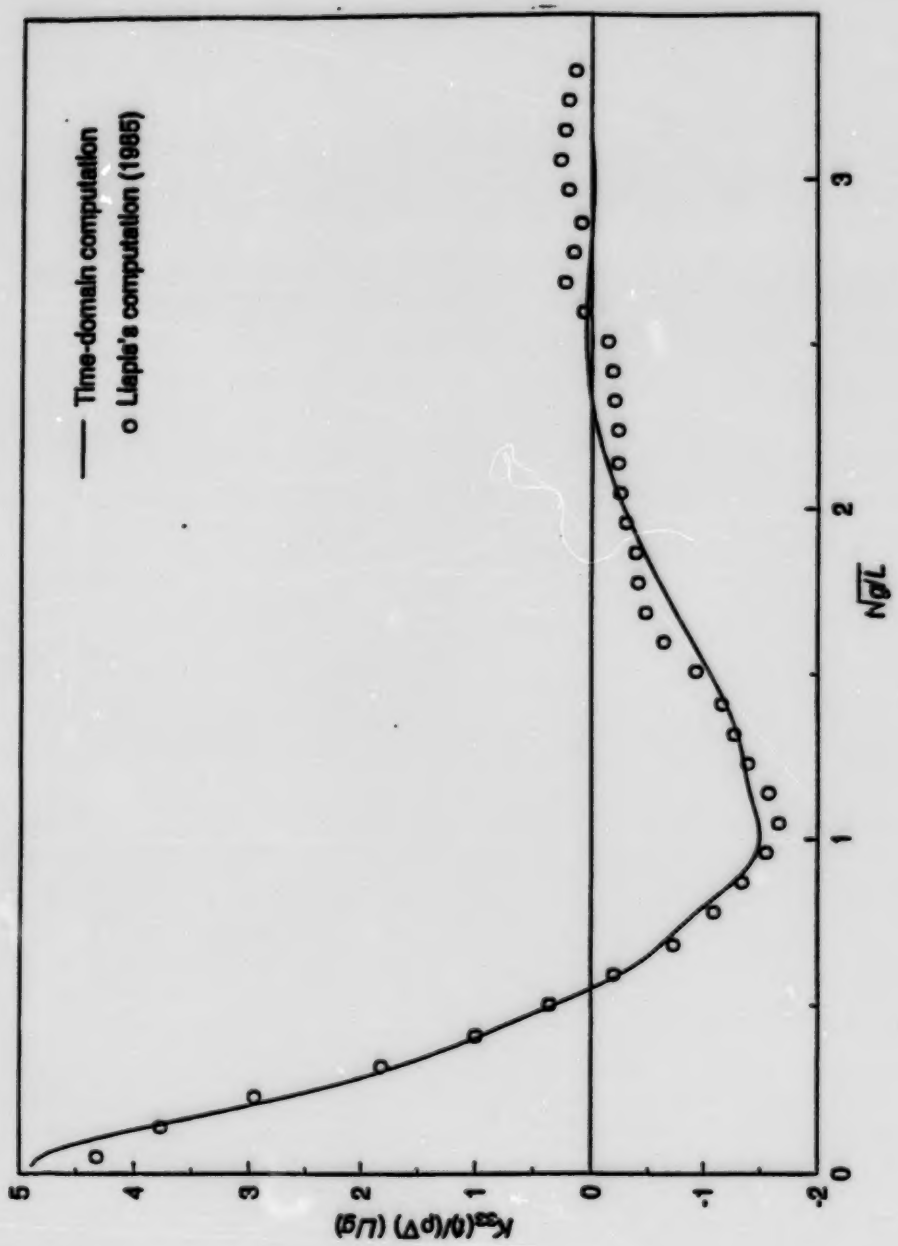

Figure 6: Response function $K_{33}(t)$ of a Series 60, $C_B = 0.7$ ($F_n = 0$)

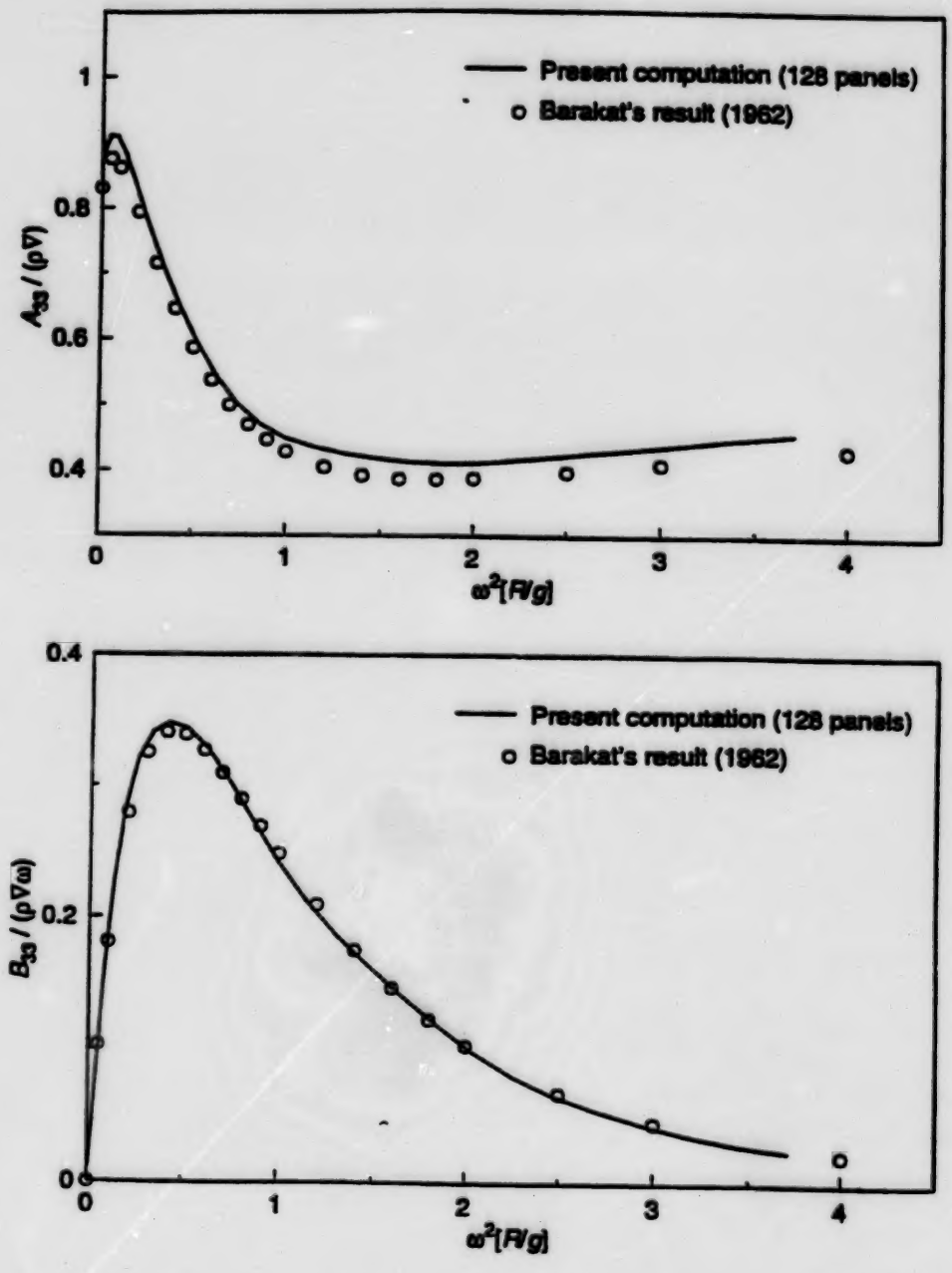

Figure 7: Added mass and damping coefficient for Series 60, $C_B = 0.7$ ($F_n = 0$)

3.3 Forces due to Diffracted Waves

The time history of free surface elevation of irregular waves can be represented by the superposition of sinusoidal waves of all frequencies with random phases. For a given wave spectrum $S_{\zeta\zeta}(\omega)$, the wave elevation is expressed as below:

$$\zeta_i(X,Y,t) = \sum_{j=1}^{\infty} \zeta_a(\omega_j)\cos(k_j X\cos\beta + k_j Y\sin\beta - \omega_j t + \varepsilon_j), \tag{75}$$

where the amplitude of the jth component wave is given by

$$\zeta_a(\omega_j) = \sqrt{2S_{\zeta\zeta}(\omega_j)(\omega_j - \omega_{j-1})}, \tag{76}$$

the random phase angle ε_j has a uniform distribution over $[0, 2\pi]$, and the wave number is $k_j = \omega_j^2/g$, and β is the wave direction.

It is desired to express the velocity field of the incident waves by using the impulse response function. In terms of the impulse response function, the velocity field can be expressed as:

$$\nabla\Phi_I(P,t) = \int_{-\infty}^{\infty} \vec{K}_v(P, t-\tau)\zeta_0(\tau)d\tau. \tag{77}$$

For the incident wave of a unit amplitude at the origin of the ship-fixed coordinate system, $\zeta_0(t) = e^{i\omega_e t}$, we have

$$\Phi_I(P,t) = \frac{ig}{\omega} e^{k(z_m - i\bar{\omega})} e^{i\omega_e t}, \tag{78}$$

and

$$\nabla\Phi_I(P,t) = \begin{pmatrix} \cos\beta \\ \sin\beta \\ i \end{pmatrix} \omega e^{k(z_m - i\bar{\omega})} e^{i\omega_e t}. \tag{79}$$

where

$$\bar{\omega} = x\cos\beta + y\sin\beta, \tag{80}$$

and

$$\omega_e = \omega + \frac{\omega^2}{g}U \tag{81}$$

From equations (77) and (79), the response function can be found as:

$$\vec{K}_v(P,t) = \frac{1}{\pi} Re\{ \begin{pmatrix} \cos\beta \\ \sin\beta \\ i \end{pmatrix} \int_0^{\infty} \omega e^{k(z_m - i\bar{\omega})} e^{i\omega_e t} d\omega_e \}. \tag{82}$$

Similarly, the incident wave field can be expressed by:

$$\zeta_I(P,t) = \int_{-\infty}^{\infty} K_\zeta(P, t-\tau)\zeta_0(\tau)d\tau, \tag{83}$$

where

$$K_\zeta(P) = e^{-ik\bar{\omega}}. \tag{84}$$

The potential function of the diffracted waves can be solved in the same way as the potential function of radiated waves by using the following body surface boundary condition:

$$\frac{\partial \phi_7}{\partial n} = -\vec{n} \cdot \nabla \Phi_I. \tag{85}$$

Substituting (77) and (82) into (85), we can express the boundary conditions of the diffracted waves for any type of incident waves in terms of the wave elevation at the origin.

The linear diffraction force is

$$F_{i7}(t) = \int\int_S p_d(P,t) n_i(P) dS, \tag{86}$$

where

$$p_d(P,t) = -\rho \frac{\partial \phi_7}{\partial t} - \rho \vec{W} \cdot \nabla \phi_7. \tag{87}$$

With the assumption of a linear system, the forces of diffracted waves can be written in the following form:

$$F_{i7}(t) = \int_{-\infty}^{\infty} K_{i7}(t-\tau)\zeta_0(\tau) d\tau, \tag{88}$$

where $\zeta_0(t)$ is the free surface elevation of incident waves at the origin of the moving coordinate system, and K_{i7} is the impulse response functions for the the diffraction force. Before the incident waves arrive at the origin, they have touched the ship hull first, hence K_{i7} is not zero for $t < 0$. Using expression (88), the diffraction force will be obtained if any type of incident wave elevation is given at the origin.

In order to obtain the response function $K_{i7}(t)$, we choose a specified non-impulse incident wave at the origin as follows:

$$\zeta_0(t) = \frac{1}{\pi} Re\{\int_0^{\infty} e^{-\omega^2/4\pi} e^{i\omega_e t} d\omega_e\}. \tag{89}$$

Similar to the radiation forces, the diffraction force can also be expressed as:

$$F_{i7}(t) = -\dot{g}_{i7}(t) - h_{i7}(t), \tag{90}$$

where

$$g_{i7}(t) = \rho \int\int_S \phi_7 n_i dS, \tag{91}$$

$$h_{i7}(t) = -\rho \int\int_S \phi_7 m_i dS - \rho \oint_\Gamma \phi_7 (\vec{l} \times \vec{n}) \cdot \vec{W} n_i d\eta. \tag{92}$$

Letting (88) equal to (90), we have

$$\int_{-\infty}^{\infty} K_{i7}(t-\tau)\zeta_0(\tau) d\tau = -\dot{g}_{i7}(t) - h_{i7}(t). \tag{93}$$

In the above expressions, only the potential function values are used in computing the diffraction forces. The solution of the kernel function K_{i7} is determined by solving the Fredholm integral equation of the first kind (93). This equation is similar to (73). The only difference here is that the integration interval is $(-\infty, \infty)$, not $(0, t)$ as in the case of radiated waves. Hence, the response function K_{i7} can be solved with the same numerical scheme, namely the method of direct solution.

The computed response functions, $K_{27}(t)$ and $K_{37}(t)$, for a hemi-sphere of radius 5 m are compared with Beck and King's results (1989) in Fig.8.

In the present method, hydrodynamic forces are expressed as the convolution products of a response kernel with either the velocity of ship motion in a given mode or the wave elevation. For example, the convolution kernels for the radiation forces are obtained for each of the six modes of motion by numerically solving the Fredholm integral equation of the first kind. The radiation response function K_{ij} needs to be solved only for a relatively short period of time for the impulsive input motion. The computation of response functions of radiated and diffracted waves were designed as two independent modules in SEALOADS. Once these two modules are run, the Green function does not need to be evaluated in the process of solving the equations of ship motion. Thus, the most time-consuming calculations of the time-domain Green function need to be done only for a relatively short period of time.

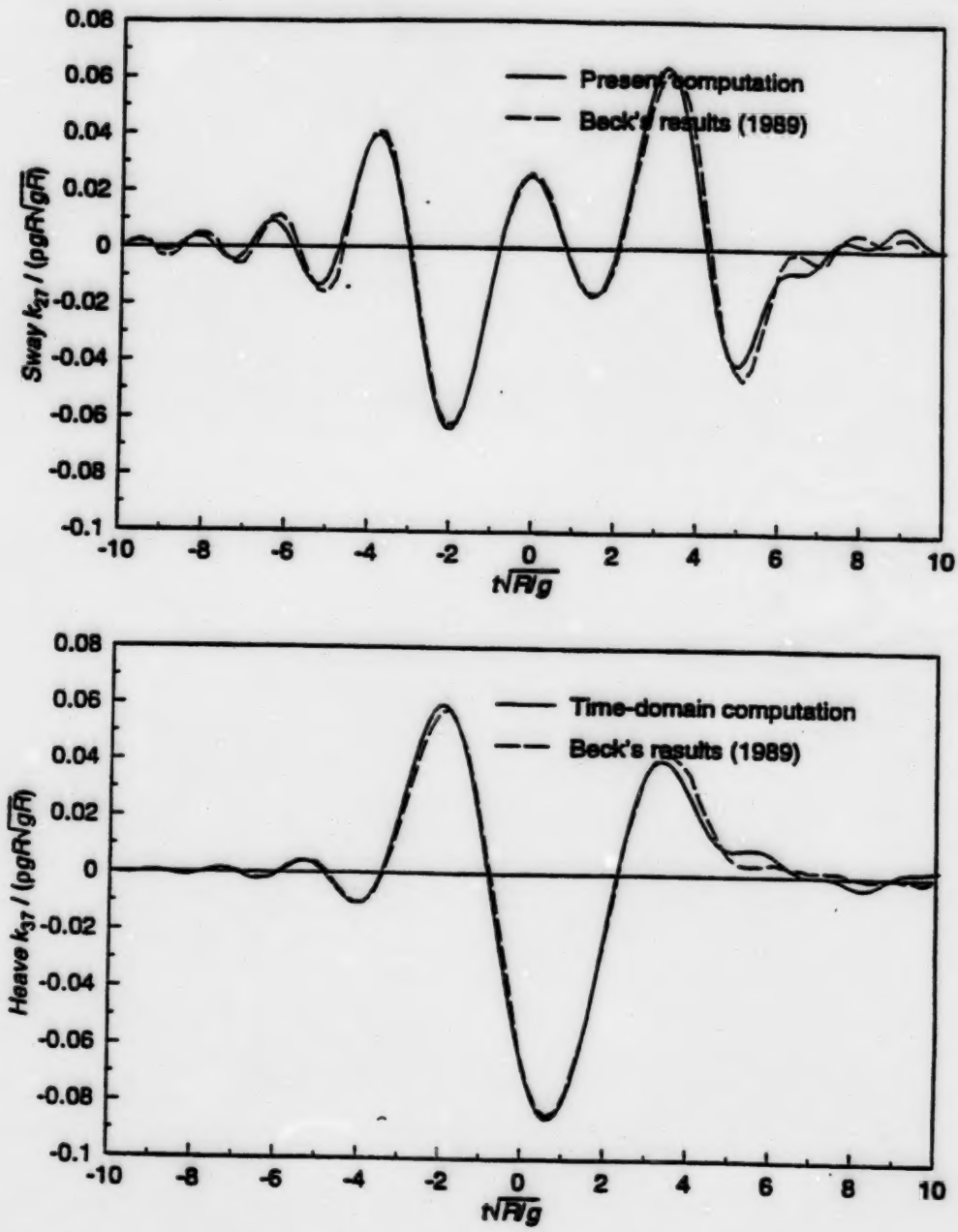

Figure 8: Response function $K_{27}(t)$ and $K_{37}(t)$ for a hemisphere ($F_n = 0$)

4 Code Structure of SEALOADS

The computer program SEALOADS for prediction of nonlinear motions, pressure distribution, and sea loads on a ship hull in large waves, consists of three main modules:

(1) radiation module;

(2) diffraction module; and

(3) motion, pressure and sea loads module.

The radiation module depends on the forward speed only. Both the response functions for the radiation forces and the pressures on each panel are solved in this module. The diffraction module depends on the forward speed and the wave heading. Also both the response functions for the diffraction forces and the pressures on each panel are solved in the module. Based on the outputs from these two modules, the ship motion and pressure distribution, and hence the sealoads can be computed for the various wave heights in regular and irregular waves. Therefore the computational time is reduced.

The code structure for SEALOADS is shown in Fig.9. Details of the flow charts for each module are shown in Figs.10, 11, and 12, respectively.

Radiation Module
Output retardation function:
1) radiation forces: $K_{ij}(t)$, $K_{ij}^{f}(t)$
2) radiation pressure: $K_{pij}(x,t)$
Diffraction Module
Output retardation function:
1) diffraction forces: $K_{i7}(t)$, $K_{i7}^{f}(t)$
2) diffraction pressure: $K_{p7}(x,t)$
Ship Motion, pressure and Sealoads Module
Output:
Time histories of ship motions, pressure and Sealoads;
Results of statistical analysis.

Fig. 9 Main Modules of SEALOADS

Radiation Force Module

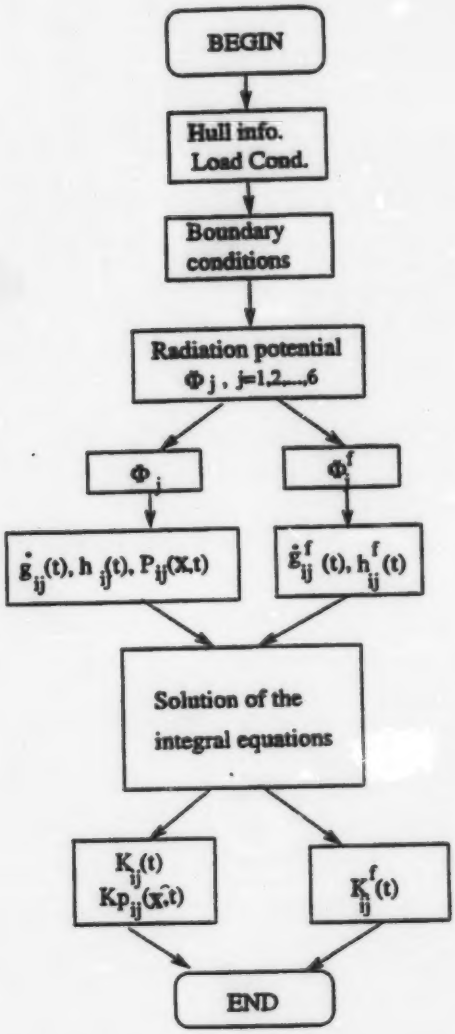

Fig. 10 Flow Chart of Radiation Module

Diffraction Force Module

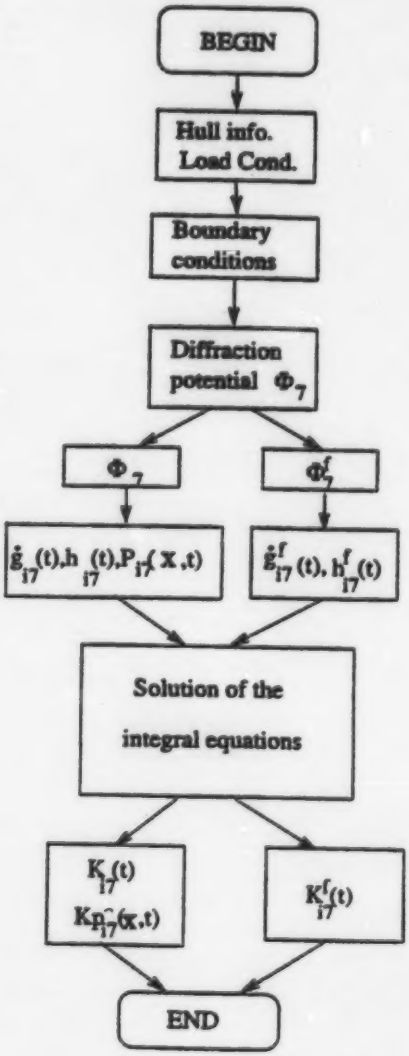

Fig. 11 Flow Chart of Diffraction Module

Flow Chart of Motion and Seaload Module

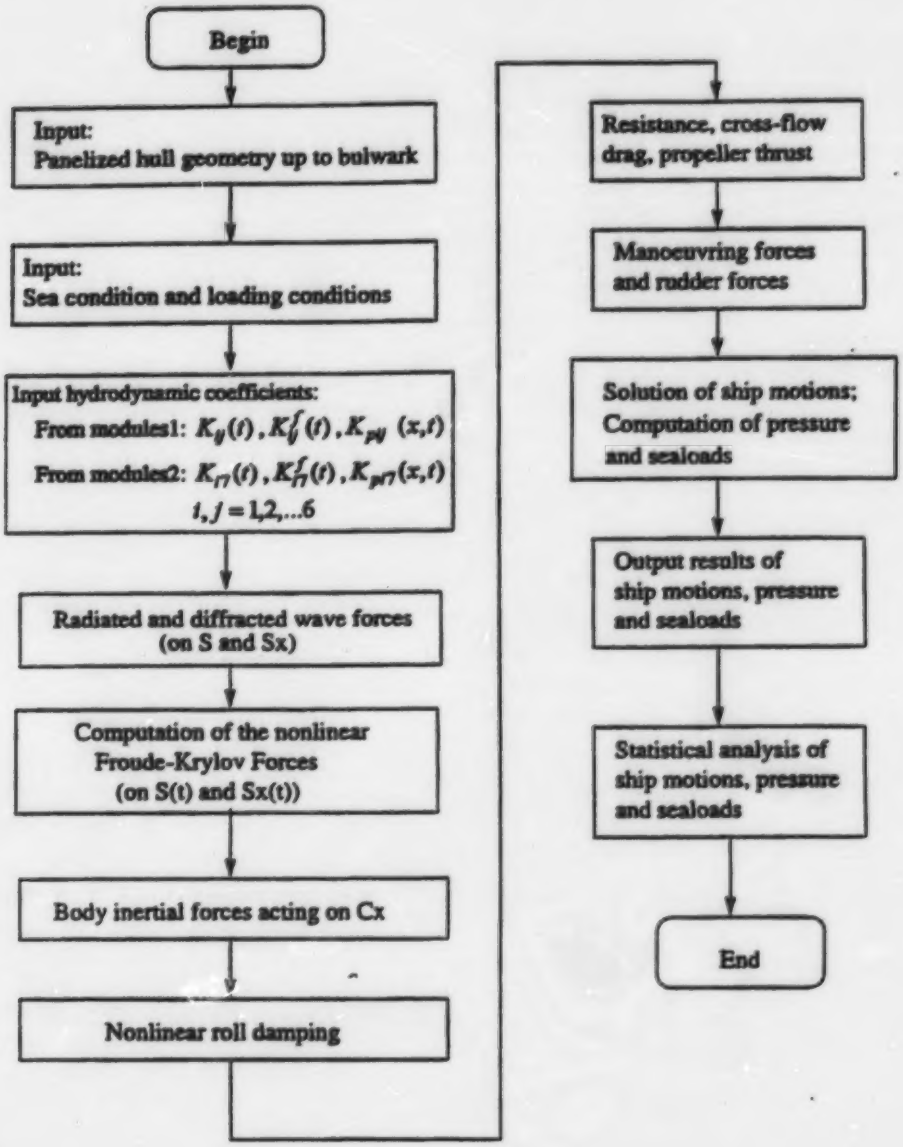

Fig. 12 Flow Chart of Motion, Pressure and Seaload Module

5 Pressure on Ship Hull

When the radiation and diffraction potentials are solved, the Bernoulli's equation can then be used to compute the pressure distribution on the hull surface, which can be decomposed as follows:

$$p(P,t) = p_i(P,t) + p_r(P,t) + p_d(P,t) \tag{94}$$

where $p_i(P,t)$ is the pressure due to incident waves, $p_r(P,t)$ is the pressure due to radiated waves, and $p_d(P,t)$ is the pressure due to diffracted waves.

5.1 Pressure induced by incident waves

In an incident wave field, the wave profile $\zeta_i(X,Y,t)$ can be computed at all nodal points on the ship hull. The vertical coordinate Z of nodal points on the wetted hull surface is compared with the incident wave surface. If a nodal point is below the wave surface $\zeta_i(X,Y,t)$, then the pressure at this point is computed by:

$$p_i(P,t) = p_{is}(P,t) + p_{id}(P,t) \tag{95}$$

where the static pressure is:

$$p_{is}(P,t) = -\rho g[Z - \zeta_i(X,Y,t)] \tag{96}$$

and the dynamic pressure is:

$$p_{id}(P,t) = -\rho\frac{\partial\Phi_i(P,t)}{\partial t} - \frac{1}{2}\rho|\nabla\Phi_i(P,t)|^2 \tag{97}$$

In this work, quadrilateral panels are used to discretize the ship-hull surface. It is assumed that at the instant t_n, there are $N(t_n)$ wetted panels on the hull surface. The mean pressure on a panel is:

$$\bar{p} = \frac{1}{4}\sum_{k=1}^{4} p_k(X,Y,Z,t) \tag{98}$$

where $p_k(X,Y,Z,t)$ is the pressure at the k^{th} nodal point of the panel. During the time integration of ship motion, the pressure $p_i(X,Y,Z,t)$ due to incident waves can be computed simultaneously with the ship motion displacement.

5.2 Pressure induced by radiated waves

In this section, we consider the hydrodynamic pressure due to the radiated waves which are generated by a ship oscillating in calm water. As it is assumed that the ship undergoes a

small amplitude motion $\eta_j(t)$ in the j^{th} mode. Then, the radiation potential can be written in terms of 6 components per unit respective motion as:

$$\phi_r(P,t) = \sum_{j=1}^{6} \phi_j(P,t) \tag{99}$$

where $\phi_j(P,t)$ is the known function solved from equation (56). Then, the Bernoulli's equation can be used to compute the pressure distribution of radiated waves. After the higher order terms are neglected, we can write:

$$p_{rj}(P,t) = -\rho\frac{\partial \phi_j}{\partial t} - \rho\vec{W}\cdot\nabla\phi_j, \qquad j = 1,2,\ldots,6 \tag{100}$$

where $\vec{W} = \nabla\bar{\phi}$, the disturbance velocity due to the steady forward speed of the ship.

For a linear system, such as the ship radiation problem, the relationship between the output pressure $p_{rj}(P,t)$ and the input motion $\eta_j(t)$ can be written as:

$$p_{rj}(P,t) = \int_0^t K_{prj}(P,t-\tau)\eta_j(\tau)d\tau, \qquad j = 1,2,\ldots,6 \tag{101}$$

Equation (101) is the Fredholm integral equation of the first kind which includes the unknown response function $K_{prj}(P,t)$. The response function $K_{prj}(P,t)$ can be solved by the so-called method of direct solution which was used to solve the radiation response function $K_{kj}(p,t)$ in Chapter 3. For more details, the method of direct solution is discussed as follows. In order to discretize equation (101) in the time domain, we use the following transformation:

$$\begin{cases} P_l &= (x_l, y_l, z_l) \\ t_m &= m\Delta t \\ \tau_n &= n\Delta\tau \end{cases}$$

then, for the motion in the jth mode and the lth panel, (101) at $t = t_m$ can be reduced to the following numerical form:

$$(p_{rjl})_m = \sum_{n=1}^{m-1}(K_{prjl})_{m-n}(\eta_j)_n\Delta t + \frac{1}{2}[(K_{prjl})_m(\eta_j)_0 + (K_{prjl})_0(\eta_j)_m]\Delta t, \qquad m = 1,\ldots,M \tag{102}$$

where M is the total number of time steps defined by $t_M = M\Delta t$. With simplified notations:

$$\begin{cases} a_m &= \eta_{jm}, \\ x_m &= (K_{prjl})_m, \\ b_m &= (p_{rjl})_m \end{cases}$$

Equation (102) becomes a system of equations in terms of x_m, or the pressure response function $(K_{prjl})_m$ at point P_l and the time instant $t_m = m\Delta t$:

$$\begin{cases} \frac{1}{2}a_1x_0 + \frac{1}{2}a_0x_1 & & & & & & & = \frac{b_1}{\Delta t} \\ \frac{1}{2}a_2x_0 + a_1x_1 + \frac{1}{2}a_0x_2 & & & & & & & = \frac{b_2}{\Delta t} \\ \cdots & & & & & & & = \cdots \\ \frac{1}{2}a_Mx_0 + a_{M-1}x_1 + \cdots & & + a_1x_{M-1} & + & \frac{1}{2}a_0x_M & & & = \frac{b_M}{\Delta t} \end{cases} \tag{103}$$

It is evident that the systems of equations (103) are indeterminate, because the total number of unknowns M is larger than the total number of equations by 1. Thus an additional physical condition has to be supplied to make (103) closed. When time $t_m = m\Delta t$ is sufficiently long, the response function $(K_{prjl})_m$ becomes quite smooth and uniformly goes to zero. Hence, a linear condition for $(K_{prjl})_m$ at a specific time instant can be supplied to (103) as the following:

$$x_{n-1} - 2x_n + x_{n+1} = 0.0 \tag{104}$$

According to our experience, setting N to a value between $M/2$ and $3M/4$ will result in a stable solution.

After (103) together with (104) are solved, the response function (K_{prjl}) becomes known and can be substituted into (101) to compute the pressure distribution due to radiation waves according to the time-series displacement of motion $\eta_j(t)$ which is obtained from the solution of time-domain equation of motion. The pressure including all modes of motion is then computed by:

$$p_r(P,t) = \sum_{j=1}^{6} p_{rj}(P,t) \tag{105}$$

5.3 Pressure induced by diffracted waves

After the diffraction potential ϕ_7 is solved, the time fluctuation of pressure $p_d(P,t)$ due to the diffracted waves can be computed by

$$p_d(P,t) = -\rho\frac{\partial\phi_7}{\partial t} - \rho\vec{W}\cdot\nabla\phi_7. \tag{106}$$

Similar to equation (101), the pressure due to the diffraction waves is also can be defined as the convolution product of the response function K_{pd} and the wave elevation at the origin of the ship-fixed coordinate system ζ_0 as follows:

$$p_d(P,t) = \int_{-\infty}^{\infty} K_{pd}(P,t-\tau)\zeta_0(\tau)d\tau. \tag{107}$$

Then, the response function of diffraction pressure $K_{pd}(P,t)$ can be solved by the method of direct solution used to solve the response function of radiation pressure. The only difference here is that the integration interval is $(-\infty,\infty)$, not $(0,t)$ as in the case of radiated waves.

With computed $K_{pr}(P,t)$ and $K_{pd}(P,t)$ previously discussed, together with the time-series motion displacement of the ship $\eta(t)$, and the incident wave at the origin $\zeta_0(t)$, the total pressure distribution due to radiated and diffracted waves can be computed by (101), (105), and (107), respectively. Finally, by adding the pressure due to incident waves (95), the total pressure can be computed by (94).

6 Sea Loads

Once we have obtained the hydrodynamic forces on the ship hull and the ship motion in the time domain, it is straightforward to compute the sea loads. Sea loads consist of two parts: one is the static load which is the difference between the weight distribution and the buoyancy distribution of the ship at the rest position in calm water, and the other part is the dynamic sea load which is due to body inertial forces, restoring forces, and hydrodynamic forces. In the time-domain simulation, we are only interested in the dynamic sea load. The vertical shear force F_S and the vertical bending moment M_B for a cross section at $x = x_c$ are given by:

$$\begin{aligned} F_S &= F_I - F_P \\ M_B &= M_I - M_P \end{aligned} \tag{108}$$

where, F_I and M_I are inertial force components, acting on the cross section at x_c, F_P and M_P are forces including all other hydrodynamic components, i.e. the restoring and Froude-Krylov forces, radiation and diffraction forces. This hydrodynamic component of sea loads can be computed by the direct integration of the pressure over the hull portion forward of x_c. Impact loads are not included in this work.

The inertial force components are computed as follows:

$$\begin{aligned} F_I &= m_{cx}\dot{u}_3 - m_{cx}(x_g - x_G)\dot{u}_5 \\ M_I &= m_{cx}(x_g - x_c)\dot{u}_3 - m_{cx}r_{xx}[r_{xx} - (x_c - x_G)]\dot{u}_5 \end{aligned} \tag{109}$$

where m_{cx} is the mass of the portion of the ship between the bow and the cross section x_c, x_g and x_G are the x coordinates of the centres of gravity of the ship segment forward of x_c and of the whole ship, respectively; and r_{xx} is the radius of gyration of the portion of the ship forward of x_c.

At each time step, the wetted panels on the hull forward of x_c are selected based on the ship displacement and the incident wave profile. After all components of hydrodynamic pressures are computed in terms of equation (94) on the whole hull surface, the sea loads due to the hydrodynamic pressure can be calculated by the direct integration of the pressure over the hull portion between bow and x_c:

$$\begin{aligned} F_P(\hat{t}) &= \int_{S_F} p_t(P,t) n_3 dS \\ M_P(t) &= \int_{S_F} p_t(P,t) n_3 (x_p - x_c) dS \end{aligned} \tag{110}$$

where S_F is the surface of the hull between the bow and the cross section at x_c, n_3 is the z component of the normal vector, while x_p is the x coordinate of the hull point P.

7 Conclusions

In this work, a time-domain methodology for predicting ship motions, hydrodynamic pressure and sea loads in waves has been developed. Nonlinear effects of the ship motions in large amplitude waves are considered in the Froude-Krylov forces, roll damping forces, cross-flow drag, manoeuvring forces, and rudder forces. The linear assumption is applied to the forces, due to the radiated and diffracted waves. The nonlinear ship motions are solved in the time domain, along with the pressure distribution and sealoads on the ship hull.

In this work, the Fredholm integral equations of the first kind for the impulse response functions of the radiated and diffracted waves were solved directly in the time domain. The impulse response functions for pressures due to both radiated and diffracted waves are also developed to predict the pressure distribution on the hull.

By this method, we were able to successfully overcome the numerical difficulties that would attend the commonly used Fourier transformation method. The computational demand of the time-domain simulation of ship motions and hull pressure distributions were significantly reduced by the present approach, so that a personal computer could be used. Nonlinear sea loads were computed by the direct surface integration of the hydrodynamic pressure distribution on the ship hull.

Generally speaking, the agreement between computed and experimental results is promising, except for the pressures at middle and afterbody. Work to improve the code is on-going. Further validation will be carried out for different wave conditions ship speeds, and for irregular waves.

Appendix A: The Radiation and Diffraction Problems

General Statement of the Problem

Considering that the fluid is incompressible and inviscid, and the flow is irrotational, in the space-fixed system the total velocity potential can be decomposed as:

$$\Phi_T(P_0,t) = \Phi_I(P_0,t) + \Phi(P_0,t) \tag{111}$$

and

$$\Phi(P_0,t) = \bar{\phi}(P_0,t) + \phi(P_0,t) \tag{112}$$

where Φ_I is the incident wave potential and Φ is the total disturbance potential. The total disturbance potential satisfies the following conditions:

$$\nabla^2\Phi(P_0,t) = 0 \tag{113}$$

$$\frac{\partial^2\Phi}{\partial t^2} + g\frac{\partial\Phi}{\partial z} = 0 \quad \text{on} \quad z = 0, \tag{114}$$

$$\frac{\partial\Phi}{\partial n} = \vec{V}_s \cdot \vec{n} - \frac{\partial\Phi_I}{\partial n} \qquad \text{on} \qquad S_i(t) \tag{115}$$

$$\nabla\Phi \to 0 \qquad \text{as} \qquad R \to \infty \qquad \text{on} \qquad z = 0 \tag{116}$$

$$\nabla\Phi \to 0 \qquad \text{as} \qquad z \to -\infty \tag{117}$$

and the initial conditions:

$$\Phi \to 0 \qquad \text{and} \qquad \frac{\partial\Phi}{\partial t} \to 0, \qquad \text{as} \qquad t \to -\infty. \tag{118}$$

where $S_i(t)$ is the transient wetted surface; $z = 0$ defines the free surface; and $R = \sqrt{x^2 + y^2}$. Equations (113) to (118) define a velocity potential caused by the motion of a floating body. The motion could be the oscillation about the mean position of the body, or the arbitrary horizontal excursion, or the combination of both. The only restriction is the linearized free surface condition (114). When the ship has a constant forward speed U in the X-direction, it is easier to treat the above problem in the moving coordinate system $o_m x_m y_m z_m$. The disturbance potential describing the absolute flow motion in a moving coordinate system becomes

$$\Phi(P,t) = \bar{\phi}(P) + \phi(P,t) \tag{119}$$

In the ship motion problem, the steady disturbance potential $\bar{\phi}$ is supposed to be known and only the unsteady disturbance potential ϕ will be discussed.

When a ship is with a steady forward speed, the complete free surface boundary condition and the body surface boundary condition for the linearized unsteady velocity potential can be derived in terms of the moving coordinate system as follows (see Newman (1978)):

$$-\frac{\phi_t+\vec{W}\cdot\nabla\phi}{g+\vec{W}\cdot\vec{W}_{z_m}}\{\frac{1}{2}\frac{\partial}{\partial z}[\vec{W}\cdot\nabla(|\vec{W}|^2)]+g\bar{\phi}_{z_mz_m}\}+\phi_{tt}+2\vec{W}\cdot\nabla\phi_t+$$

$$+\vec{W}\cdot\nabla(\vec{W}\cdot\nabla\phi)+\frac{1}{2}\nabla\phi\cdot\nabla(|\vec{W}|^2)+g\phi_{z_m}=0 \qquad \text{on} \qquad z=\bar{\zeta} \tag{120}$$

$$\frac{\partial\phi}{\partial n}=[\vec{\alpha}_t+(\vec{W}\cdot\vec{\nabla})\vec{\alpha}-(\vec{\alpha}\cdot\nabla)\vec{W}]\cdot\vec{n}-\frac{\partial\Phi_I}{\partial n} \qquad \text{on} \qquad \bar{S}. \tag{121}$$

where $\bar{\zeta}$ is the steady free-surface elevation and $\vec{\alpha}_t$ denotes the time differentiation of the local oscillatory displacement of the ship's surface. The influence from the steady wave system is included in the above formulae and there is no restriction on the shape of the ship hull. In equation (121), the second term in the square brackets represents the contribution from the steady wave system and the ship angular oscillations, and the third term is the contribution due to the gradient of flow of the steady wave system. An alternative expression of (121) can be given, as in the paper of Ogilvie and Tuck (1969) and Newman (1978), as follows:

$$\frac{\partial\phi}{\partial n}=\sum_{j=1}^{6}(\frac{\partial\eta_j}{\partial t}n_j+\eta_jm_j)-\frac{\partial\Phi_I}{\partial n} \qquad \text{on} \qquad \bar{S}. \tag{122}$$

Radiated and Diffracted Wave Potentials

There is no elementary solution for the above problem, and we have to separate the unsteady wave system which is due to the oscillatory ship motion from the steady wave system which is due to the ship advancing at a constant forward speed in calm water. Under the assumption of infinitesimal steady waves, which implies the slender ship hull and slow forward speed, the boundary conditions corresponding to (120) and (121) can be simplified as follows:

$$(\frac{\partial}{\partial t}-U\frac{\partial}{\partial x_m})^2\phi+g\phi_z=0 \qquad \text{on,} \qquad z_m=0 \tag{123}$$

$$\frac{\partial\phi}{\partial n}=[(\frac{\partial}{\partial t}-U\frac{\partial}{\partial x})\vec{\alpha}]\cdot\vec{n}-\frac{\partial\Phi_I}{\partial n} \qquad \text{on} \qquad \bar{S}, \tag{124}$$

where the steady waves have no effect on the unsteady waves.

Equations for the linearized unsteady disturbance velocity potential $\phi(P,t)$ can be expressed as follows:
the governing equation (Laplace's equation):

$$\nabla^2\phi(P,t)=0, \tag{125}$$

the free surface condition:

$$(\frac{\partial}{\partial t} - U\frac{\partial}{\partial x_m})^2\phi + g\frac{\partial \phi}{\partial z_m} = 0 \qquad \text{on} \qquad z_m = 0, \tag{126}$$

the boundary condition on the wetted hull surface:

$$\frac{\partial \phi}{\partial n} = \vec{V}_s \cdot \vec{n} - \frac{\partial \Phi_I}{\partial n} \qquad \text{on} \qquad \bar{S}, \tag{127}$$

the far field condition:

$$\nabla\phi \to 0 \qquad \text{as} \qquad R \to \infty \qquad \text{on} \qquad z_m = 0, \tag{128}$$

$$\nabla\phi \to 0 \qquad \text{as} \qquad z_m \to -\infty, \tag{129}$$

and the initial conditions:

$$\phi \to 0 \qquad \text{and} \qquad \frac{\partial \phi}{\partial t} \to 0, \qquad \text{as} \qquad t \to -\infty. \tag{130}$$

The above unsteady disturbance velocity potential can be further decomposed as follows:

$$\phi(P,t) = \phi_R(P,t) + \phi_7(P,t) = \sum_{j=1}^{6} \phi_j(P,t) + \phi_7(P,t). \tag{131}$$

The radiation potential ϕ_R is due to six modes of oscillation in the steady flow field and the diffraction potential ϕ_7 is due to the presence of the body in the incident wave field. The body surface boundary conditions are:

$$\frac{\partial \phi_R}{\partial n} = \sum_{j=1}^{6} (\frac{\partial \eta_j}{\partial t} n_j + \eta_j m_j) \qquad \text{on} \qquad \bar{S}, \tag{132}$$

and

$$\frac{\partial \phi_7}{\partial n} = -\frac{\partial \Phi_I}{\partial n} \qquad \text{on} \qquad \bar{S}. \tag{133}$$

From equations (125) to (133), the initial-boundary value problem for the radiation potential, $\phi_j, j = 1, 2, \cdots, 6$, and the diffraction potential, $j = 7$, are as follows:

$$\nabla^2\phi_j(P,t) = 0 \qquad \text{in fluid domain,} \tag{134}$$

the free surface condition:

$$(\frac{\partial}{\partial t} - U\frac{\partial}{\partial x_m})^2\phi_j + g\frac{\partial \phi_j}{\partial z_m} = 0 \qquad \text{on} \qquad z_m = 0, \tag{135}$$

the boundary condition on the wetted hull surface $\bar{S}$:

$$\frac{\partial \phi_j}{\partial n} = \begin{cases} \frac{\partial \eta_j}{\partial t} n_j + \eta_j m_j & \text{for } j = 1, 2, \cdots, 6, \\ -\frac{\partial \Phi_I}{\partial n} & \text{for } j = 7, \end{cases} \tag{136}$$

the far-field conditions:

$$\nabla \phi_j \to 0 \quad \text{as} \quad R \to \infty \quad \text{on} \quad z_m = 0$$

$$\nabla \phi_j \to 0 \quad \text{as} \quad z_m \to -\infty$$

and the initial conditions:

$$\phi_j \to 0 \quad \text{and} \quad \frac{\partial \phi_j}{\partial t} \to 0, \quad \text{as} \quad t \to -\infty$$

The m-terms in (136) can be expressed as follows:

$$\vec{W} = -\vec{i}U + \nabla \bar{\phi}, \tag{137}$$

$$(m_1, m_2, m_3) = -(n_1 \frac{\partial}{\partial x_m} + n_2 \frac{\partial}{\partial y_m} + n_3 \frac{\partial}{\partial z_m})(W_1, W_2, W_3), \tag{138}$$

and

$$\begin{aligned} (m_4, m_5, m_6) \;=\; & -(n_1 \frac{\partial}{\partial x_m} + n_2 \frac{\partial}{\partial y_m} + n_3 \frac{\partial}{\partial z_m}) \\ & \cdot (y_m W_3 - z_m W_2, z_m W_1 - x_m W_3, x_m W_2 - y_m W_1), \end{aligned} \tag{139}$$

where $\bar{\phi}$ can be obtained from the steady wave potential in the wave resistance theory or from the double-body flow approximation. When the steady wave potential $\bar{\phi}$ is assumed to be a small quantity, the steady velocity field is approximated by:

$$\vec{W} = -\vec{i}U, \tag{140}$$

and the m-terms are as follows:

$$(m_1, m_2, m_3) = (0, 0, 0), \tag{141}$$

$$(m_4, m_5, m_6) = (0, Un_3, -Un_2). \tag{142}$$

As discussed above, the simplified m-terms in (141) and (142) may cause errors in the motion computation.

Computation of m-terms

In order to provide the boundary condition for the potential χ_j and to compute the hydrodynamic damping and hydrodynamic restoring coefficients, the m-terms have to be calculated. The computation is related to the second derivatives of the steady flow potential. It is difficult to obtain an acceptable second derivative by direct numerical differentiation if flat panels with a constant source are used. To avoid the direct evaluation of the second derivatives, an integral equation method has been applied to the 2-D body by Wu (1991) and extended to 3-D body by Huang and Hsiung (1993a) based on double-body flow.

The definition of the m-terms are as follows:

$$(m_1, m_2, m_3) = -(\vec{n} \cdot \nabla)\vec{W} = (\frac{\partial^2}{\partial n \partial x_m}, \frac{\partial^2}{\partial n \partial y_m}, \frac{\partial^2}{\partial n \partial z_m})\vec{W}, \tag{143}$$

$$(m_4, m_5, m_6) = -(\vec{n} \cdot \nabla)(\vec{r} \times \vec{W}), \tag{144}$$

or

$$\begin{aligned} m_4 &= n_2 W_3 - n_3 W_2 + y m_3 - z m_2, \\ m_5 &= n_3 W_1 - n_1 W_3 + z m_1 - x m_3, \\ m_6 &= n_1 W_2 - n_2 W_1 + x m_2 - y m_1, \end{aligned}$$

where $\vec{W} = (W_1, W_2, W_3)$ is the velocity vector in the steady flow field around the advancing ship. The steady flow is induced by the advancing motion of the ship at a constant forward speed U in calm water. In this work, the steady flow is substituted by the so-called "double-body" flow. By introducing the Green function:

$$\bar{G} = \frac{1}{r} + \frac{1}{r_1}, \tag{145}$$

where

$$r = \sqrt{(x_m - \xi_m)^2 + (y_m - \eta_m)^2 + (z_m - \zeta_m)^2}, \tag{146}$$

$$r_1 = \sqrt{(x_m - \xi_m)^2 + (y_m - \eta_m)^2 + (z_m + \zeta_m)^2}, \tag{147}$$

and applying the Green theorem to the steady flow potential, $\bar{\Phi}$, and the Green function $\bar{G}$, the potential function $\bar{\Phi}$ can be obtained from:

$$\bar{\Phi}(\vec{x}_m) = -\frac{1}{4\pi} \int\int_S \sigma(\vec{\xi}_m) \bar{G}(\vec{x}_m, \vec{\xi}_m) dS. \tag{148}$$

where $\vec{x}_m = (x_m, y_m, z_m)$ is the field point, $\vec{\xi}_m = (\xi_m, \eta_m, \zeta_m)$ is the source point, and $\sigma(\vec{\xi}_m)$ is the source strength.

Applying the second Green theorem to $\bar{\Phi}_{x_m}$ and $\bar{G}$, the following integral equation can be obtained

$$\frac{\partial \bar{\Phi}(\vec{x}_m)}{\partial x_m} = \frac{1}{2\pi}\int\int_{S+S_f}[\frac{\partial \bar{\Phi}(\vec{\xi}_m)}{\partial \xi_m}\frac{\partial \bar{G}}{\partial n} - \bar{G}(\vec{x}_m,\vec{\xi}_m)\frac{\partial^2 \bar{\Phi}(\vec{\xi})}{\partial n \partial \xi_m}]dS. \tag{149}$$

On the free surface S_f, $\frac{\partial \bar{G}}{\partial n} = 0$ and $\frac{\partial^2 \bar{\Phi}}{\partial n \partial \xi_m} = -\frac{\partial^2 \bar{\Phi}}{\partial z_m \partial \xi_m} = 0$. Using the definition of the m-terms, we have

$$\frac{\partial \bar{\Phi}(\vec{x}_m)}{\partial x_m} = \frac{1}{2\pi}\int\int_{S}[\frac{\partial \bar{\Phi}(\vec{\xi}_m)}{\partial \xi_m}\frac{\partial \bar{G}}{\partial n} - \bar{G}(\vec{x}_m,\vec{\xi}_m)m_1(\vec{\xi}_m)]dS \tag{150}$$

in which, $\bar{\Phi}$ and $\frac{\partial \bar{\Phi}(\vec{\xi}_m)}{\partial \xi_m}$ have been solved from equation (148). From the above integral equation, m_1 can be obtained. Similarly, we can derive the following equation for m_2:

$$\frac{\partial \bar{\Phi}(\vec{x}_m)}{\partial y_m} = \frac{1}{2\pi}\int\int_{S}[\frac{\partial \bar{\Phi}(\vec{\xi}_m)}{\partial \eta_m}\frac{\partial \bar{G}}{\partial n} - \bar{G}(\vec{x}_m,\vec{\xi}_m)m_2(\vec{\xi}_m)]dS. \tag{151}$$

If the Green theorem is applied to $\frac{\partial \bar{\Phi}}{\partial z_m}$ and $\bar{G}$, we cannot eliminate the term $\bar{G}(\vec{x}_m,\vec{\xi}_m)\frac{\partial}{\partial n}\bar{\Phi}(\vec{\xi}_m)$ in the free surface integration, because $\frac{\partial \bar{\Phi}_{xm}}{\partial z_m} \neq 0$. However, the Green function can be modified to

$$\tilde{G}(\vec{x}_m,\vec{\xi}_m) = \frac{1}{r} - \frac{1}{r_1}, \tag{152}$$

so that $\tilde{G} = 0$ on the free surface. Since the potential function $\bar{\Phi}$ has already been solved for the double-body flow, we still have $\frac{\partial \bar{\Phi}}{\partial \zeta_m} = 0$ on the free surface. Therefore, the free surface integration will disappear and the integral equation for m_3 is

$$\frac{\partial \bar{\Phi}(\vec{x}_m)}{\partial z_m} = \frac{1}{2\pi}\int\int_{S}[\frac{\partial \bar{\Phi}(\vec{\xi}_m)}{\partial \zeta_m}\frac{\partial \tilde{G}}{\partial n} - \tilde{G}(\vec{x}_m,\vec{\xi}_m)m_3(\vec{\xi}_m)]dS. \tag{153}$$

Analytical formulae introduced by Hess and Smith (1967) are adopted in calculating the integral of the Rankine source over the flat panels. According to the numerical test, in order to keep the numerical results of m-terms stable, it requires that panels are evenly distributed at the location where the body surface has a large curvature.

Generally speaking, the aforementioned potentials due to the radiated and diffracted waves can be found by solving the corresponding initial and boundary problems in (125) through (130), if the computer speed is sufficiently fast and the memory capacity is sufficiently large. In time-domain simulation for a long interval, the personal computer might not be able to solve this very complicated problem. In this work, instead of directly solving the problem expressed by (125) through (130), we use the impulse function method by Cummins (1962), which is discussed in Section 3.

Appendix B: The Time-Domain Green Function

In this work, the method developed by Huang and Hsiung (1991) is used to compute the time-domain Green function. The Fast Fourier Transform is employed in the computation. When the source point and the field point are on the free surfaces, Green's function and its derivatives are expressed in analytical forms, which can be easily calculated. The numerical behavior of Green's function is studied in this work and numerical examples are presented. It shows that the present algorithm can be used in the time-domain ship hydrodynamics.

Definition of the Green Function

The initial-boundary value problem for the time-domain Green's function in 3-D was given by Wehausen and Laitone (1960) in the space-fixed coordinate system $OXYZ$. The Green function was given as follows:

$$G(P,\ Q,\ t) = G_0(P,\ Q)\delta(t) + G_f(P,\ Q,\ t)H(t) \tag{154}$$

where $H(t)$ is Heaviside function, $P = (X, Y, Z)$ is the field point, $Q = (\xi_0, \eta_0, \zeta_0)$ is the source point, in the $OXYZ$ system,

$$G_0(P,\ Q) = \frac{1}{r} - \frac{1}{r_1} \tag{155}$$

and

$$G_f(P,\ Q,\ t) = 2\int_0^\infty dk\sqrt{gk}\sin[\sqrt{gk}t]e^{k(z+\zeta)}J_0(kR) \tag{156}$$

$$r^2 = (X-\xi_0)^2 + (Y-\eta_0)^2 + (Z-\zeta_0)^2 \tag{157}$$

$$r_1^2 = (X-\xi_0)^2 + (Y-\eta_0)^2 + (Z+\zeta_0)^2 \tag{158}$$

$$R^2 = (X-\xi_0)^2 + (Y-\eta_0)^2 \tag{159}$$

In order to develop a new method to compute the Green function, $G_f(P,\ Q,\ t)$ will be expressed in a different form by the change of variables. Let

$$\lambda = kr_1, \qquad \mu = -\frac{Z+\zeta_0}{r_1}, \qquad \beta = \sqrt{\frac{g}{r_1}}t$$

then

$$kR = \sqrt{1-\mu^2}\lambda$$

$$\sqrt{gk} = \sqrt{\frac{g}{r_1}\lambda}$$

$$k(Z+\zeta_0) = -\lambda\mu$$

$$dk = \frac{1}{r_1} d\lambda$$

Hence, (156) becomes

$$\begin{aligned} G_f(P, Q, t) &= G_f(\beta, \mu) \\ &= 2\sqrt{\frac{g}{r_1^3}} \int_0^\infty d\lambda \sqrt{\lambda} \sin(\beta\sqrt{\lambda}) e^{-\lambda\mu} J_0(\sqrt{1-\mu^2}\lambda) \end{aligned} \tag{160}$$

or

$$G_f(\beta, \mu) = 2\sqrt{\frac{g}{r_1^3}} I_1(\beta, \mu) \tag{161}$$

where

$$I_1(\beta, \mu) = \int_0^\infty d\lambda \sqrt{\lambda} \sin(\beta\sqrt{\lambda}) e^{-\lambda\mu} J_0(\sqrt{1-\mu^2}\lambda) \tag{162}$$

Also, we have

$$\frac{\partial}{\partial X} G_f(P, Q, t) = -2\frac{(X-\xi_0)}{R} \int_0^\infty dk k \sqrt{gk} \sin[\sqrt{gk}t] e^{k(z-\zeta)} J_1(kR)$$

$$\frac{\partial}{\partial X} G_f(\beta, \mu) = -2\sqrt{\frac{g}{r_1^3}} \frac{(X-\xi_0)}{r_1 R} I_2(\beta, \mu) \tag{163}$$

where

$$I_2(\beta, \mu) = \int_0^\infty d\lambda \cdot \lambda \sqrt{\lambda} \sin[\beta\sqrt{\lambda}] e^{-\lambda\mu} J_1(\sqrt{1-\mu^2}\lambda) \tag{164}$$

Similarly,

$$\frac{\partial}{\partial Y} G_f(\beta, \mu) = -2\sqrt{\frac{g}{r_1^3}} \frac{(y-\eta)}{r_1 R} I_2(\beta, \mu) \tag{165}$$

$$\frac{\partial}{\partial Z} G_f(\beta, \mu) = 2\sqrt{\frac{g}{r_1^3}} \frac{1}{r_1} I_3(\beta, \mu) \tag{166}$$

where

$$I_3(\beta, \mu) = \int_0^\infty d\lambda \cdot \lambda \sqrt{\lambda} \sin[\beta\sqrt{\lambda}] e^{-\lambda\mu} J_0(\sqrt{1-\mu^2}\lambda) \tag{167}$$

In the above derivation,

$$\frac{d}{dx} J_0(x) = -J_1(x)$$

is used.

The time derivative of the Green function can be obtained from:

$$\begin{aligned} \frac{\partial}{\partial t} G_f(P, Q, t) &= \frac{\partial}{\partial t} G_f(\beta, \mu) \\ &= 2\frac{g}{r_1^2} I_4(\beta, \mu) \end{aligned} \tag{168}$$

where

$$I_4(\beta, \mu) = \int_0^\infty d\lambda \cdot \lambda \cdot \cos[\beta\sqrt{\lambda}] e^{-\lambda\mu} J_0(\sqrt{1-\mu^2}\lambda) \tag{169}$$

Integral Transform Method for $\mu \neq 0$

The Fourier sine transform of a function $f(\lambda)$ is defined as:

$$F_s(\beta) = F_s[f(\lambda)] = \int_0^\infty d\lambda \sin \beta\lambda \cdot f(\lambda) \tag{170}$$

and the Fourier cosine transform:

$$F_c(\beta) = F_c[f(\lambda)] = \int_0^\infty d\lambda \cos \beta\lambda \cdot f(\lambda) \tag{171}$$

From (163), (165) and (168), it can be seen that I_1, I_2 and I_3 are the Fourier sine transform of the following three functions, respectively:

$$g_1(\beta,\ \mu,\ \lambda) = \sqrt{\lambda} e^{-\lambda\mu} J_0(\sqrt{1-\mu^2}\lambda) \tag{172}$$

$$g_2(\beta,\ \mu,\ \lambda) = \lambda\sqrt{\lambda} e^{-\lambda\mu} J_1(\sqrt{1-\mu^2}\lambda) \tag{173}$$

and

$$g_3(\beta,\ \mu,\ \lambda) = \lambda g_1(\beta,\ \mu,\ \lambda) \tag{174}$$

These are decay functions of λ.

Equation (169) is the Fourier cosine transform of the function:

$$g_4(\beta,\ \mu,\ \lambda) = \lambda e^{-\lambda\mu} J_0(\sqrt{1-\mu^2}\lambda) \tag{175}$$

Let

$$q = \sqrt{\lambda}, \qquad (d\lambda = 2qdq)$$

then we have, from (162), (164), (167) and (169), the following:

$$I_1(\beta,\ \mu) = F_s[h_1(q)] \tag{176}$$

$$I_2(\beta,\ \mu) = F_s[h_2(q)] \tag{177}$$

$$I_3(\beta,\ \mu) = F_s[h_3(q)] \tag{178}$$

and

$$I_4(\beta,\ \mu) = F_c[h_4(q)] \tag{179}$$

where

$$h_1(q) = 2q^2 J_0(\sqrt{1-\mu^2}q^2) e^{-\mu q^2} \tag{180}$$

$$h_2(q) = 2q^4 J_1(\sqrt{1-\mu^2}q^2) e^{-\mu q^4} \tag{181}$$

$$h_3(q) = q^2 h_1(q) \tag{182}$$

$$h_4(q) = q h_1(q) \tag{183}$$

Analytical Expressions for $\mu = 0$

When $\mu = 0$, the integrands in the Green function and its spatial derivatives, at large t, oscillate very fast. Let $\omega = \frac{1}{2}\beta$, and after a lengthy manipulation, we have the following results:

$$I_1(\beta,0) = \pi\omega^3\sqrt{\frac{1}{2R}}[J_{\frac{1}{4}}(\frac{1}{2}\omega^2)J_{-\frac{1}{4}}(\frac{1}{2}\omega^2) + J_{\frac{3}{4}}(\frac{1}{2}\omega^2)J_{-\frac{3}{4}}(\frac{1}{2}\omega^2)] \tag{184}$$

$$\begin{aligned} I_2(\beta,\,0) \;=\; & \frac{\pi}{2\sqrt{2}}\{\frac{5}{2}\omega^3 J_{\frac{1}{4}}J_{-\frac{1}{4}}(\frac{1}{2}\omega^2) \\ & +\omega^5[J_{-\frac{1}{4}}J_{-\frac{3}{4}}(\frac{1}{2}\omega^2) - J_{\frac{1}{4}}J_{\frac{3}{4}}(\frac{1}{2}\omega^2)] + \frac{3}{2}\omega^3 J_{\frac{3}{4}}J_{-\frac{3}{4}}(\frac{1}{2}\omega^2)\} \end{aligned} \tag{185}$$

$$\begin{aligned} I_3(\beta,\,0) \;=\; & -\frac{\pi}{2\sqrt{2}}\{(\frac{1}{2}\omega - \omega^5)J_{\frac{1}{4}}J_{-\frac{1}{4}}(\frac{1}{2}\omega^2) \\ & -\frac{3}{2}\omega^3[J_{\frac{1}{4}}J_{\frac{3}{4}}(\frac{1}{2}\omega^2) - J_{-\frac{1}{4}}J_{-\frac{3}{4}}(\frac{1}{2}\omega^2)] - \omega^5 J_{\frac{3}{4}}J_{-\frac{3}{4}}(\frac{1}{2}\omega^2)\} \end{aligned} \tag{186}$$

$$\begin{aligned} I_4(\beta,\,0) \;=\; & -\frac{\pi}{16\sqrt{2}}\{\frac{3}{4}\omega^2 J_{\frac{1}{4}}J_{-\frac{1}{4}}(\frac{1}{2}\omega^2) \\ & +\frac{1}{32}\omega^4[J_{-\frac{1}{4}}J_{-\frac{3}{4}}(\frac{1}{2}\omega^2) - J_{\frac{1}{4}}J_{-\frac{3}{4}}(\frac{1}{2}\omega^2)]\} \end{aligned} \tag{187}$$

Numerical Computation of the Green Function

In practical computation, it is convenient to use the following expressions:

$$I_1(\beta,\mu) = e^{-\frac{\mu\rho^2}{4}}I_1(\beta,\,0) + \Delta I_1(\beta,\,\mu)$$

$$I_2(\beta,\mu) = e^{-\frac{\mu\rho^2}{4}}I_2(\beta,\,0) + \Delta I_2(\beta,\,\mu)$$

$$I_3(\beta,\mu) = e^{-\frac{\mu\rho^2}{4}}I_3(\beta,\,0) + \Delta I_3(\beta,\,\mu)$$

$$I_4(\beta,\mu) = e^{-\frac{\mu\beta^2}{4}} I_4(\beta,\ 0) + \Delta I_4(\beta,\ \mu)$$

We first establish five data blocks, one for $I_i(\beta,0)$ and four for $\Delta I_i(\beta,\mu)$ $(i=1,2,3,4)$. The data blocks are saved in five permanent data files. Therefore, we do not need to establish the data blocks again in the computation of the ship motion. There are 400 intervals in β with $\Delta\beta = 0.1$, and 30 in μ with $\Delta\mu$ unevenly distributed in each data block. In practical computation, numerical interpolation is used for $I_i(\beta,\mu)$ and $\Delta I_i(\beta,\mu)$ to reduce the computing time. The input variables are (X,Y,Z), (ξ_0,η_0,ζ_0), t and τ. Then, β and μ are computed. The term $I_i(\beta,\mu)$ $(i=1,2,3,4)$ are computed from the above formulas. The Green function and its derivative are computed as follows:

$$G_f(\beta,\ \mu) = 2\sqrt{\frac{g}{r_1^3}} I_1(\beta,\ \mu) \tag{188}$$

$$\frac{\partial}{\partial X} G_f(\beta,\ \mu) = -2\sqrt{\frac{g}{r_1^3}} \frac{(x-\xi)}{r_1 R} I_2(\beta,\ \mu) \tag{189}$$

$$\frac{\partial}{\partial Y} G_f(\beta,\ \mu) = -2\sqrt{\frac{g}{r_1^3}} \frac{(y-\eta)}{r_1 R} I_2(\beta,\ \mu) \tag{190}$$

$$\frac{\partial}{\partial Z} G_f(\beta,\ \mu) = 2\sqrt{\frac{g}{r_1^3}} \frac{1}{r_1} I_3(\beta,\ \mu) \tag{191}$$

$$\frac{\partial}{\partial t} G_f(\beta,\mu) = 2\frac{g}{r_1^2} I_4(\beta,\ \mu) \tag{192}$$

Appendix C: Numerical Solutions of the Potential Functions

The discretized Green function can be written as

$$G_{ij}^{k_t-k_\tau} = G_{0ij}\delta(k_t\Delta t - k_\tau\Delta t) + G_{fij}^{k_t-k_\tau}H[(k_t-k_\tau)\Delta t] \tag{193}$$

where the current time instant is $t_k = k_t\Delta t$, time $\tau = k_\tau\Delta t$, subscript "0" is for the Rankine source and its mirror image part in the Green function, "f" for the wave part, "i" for field points, and "j" for source points.

$$G_{0ij} = \frac{1}{r_{ij}} - \frac{1}{r_{1ij}} \tag{194}$$

$$G_{fij}^{k_t-k_\tau} = 2\int_0^\infty dk\sqrt{gk}\sin[\sqrt{gk}(k_t-k_\tau)\Delta t]e^{k(z_i+\zeta_j)}J_0(kR_{ij}) \tag{195}$$

where

$$R_{ij} = \sqrt{(x_i-\xi_j)^2+(y_i-\eta_j)^2} \tag{196}$$

$$r_{ij} = \sqrt{(x_i-\xi_j)^2+(y_i-\eta_j)^2+(z_i-\zeta_j)^2} \tag{197}$$

$$r_{1ij} = \sqrt{(x_i-\xi_j)^2+(y_i-\eta_j)^2+(z_i+\zeta_j)^2} \tag{198}$$

Suppose that the source strength on each panel is constant. Then the integral equations (56) for the radiated wave potentials can be discretized as follow:

$$\begin{aligned} -\frac{1}{2}(\sigma_J)_i^{k_t} &+ \sum_{j=1}^{N_p}(\sigma_J)_i^{k_t}I_{s0ij} + \Delta t[\frac{1}{2}\sum_{j=1}^{N_p}(\sigma_J)_j^0 I_{sfij}^{k_t} + \sum_{k_\tau=1}^{k_t-1}\sum_{j=1}^{N_p}(\sigma_J)_j^{k_\tau}I_{sfij}^{k_t-k_\tau}] \\ &+ \Delta t[\frac{1}{2}\sum_{l=1}^{N_l}(\sigma_J^L)_l^0 I_{Lfil}^{k_t} + \sum_{k_\tau=1}^{k_t-1}\sum_{l=1}^{N_l}(\sigma_J^L)_l^k I_{Lfil}^{k_t-k_\tau}] \\ &= \sqrt{\frac{\bar{a}L}{\pi g}}e^{-\bar{a}(k_t\Delta t)^2}(n_J)_i - \frac{1}{2}\sqrt{\frac{L}{g}}[1+\mathrm{erf}(\bar{a},t)](m_J)_i \end{aligned} \tag{199}$$

where $J = 1, 2, \cdots, 6$ are the modes of motion of the body, and subscript (or superscript) L denotes the physical variable on panels neighboring the waterline. In SEALOADS, the source strength and the potential function on the waterline are assumed to be equal to the values of the neighboring panels. On panels,

$$\begin{cases} I_{s0ij} = -\frac{1}{4\pi}\int\int_{\Delta S_j}(\frac{\delta G_0}{\delta n})_{ij}dS \\ I_{sfij}^{k_t-k} = -\frac{1}{4\pi}\int\int_{\Delta S_j}(\frac{\delta G_f}{\delta n})_{ij}^{k_t-k}dS \end{cases} \tag{200}$$

and along the waterline,

$$\begin{cases} I_{L0il} = -\frac{u^2}{4\pi g}\int_{\Delta L_l}(n_1)_l(\frac{\partial G_0}{\partial n})_{il}dL \\ I_{Ljil}^{k_t-k} = -\frac{u^2}{4\pi g}\int_{\Delta L_l}(n_1)_l(\frac{\partial G_j}{\partial n})_{il}^{k_t-k}dL \end{cases} \tag{201}$$

As $G_{fij}^{k_\tau-k_t}=0$ when $k_\tau=k_t$, a linear algebra system can be derived from (199):

$$\sum_{j=1}^{N_p} A_{ij}^{k_t}(\sigma_J)_j^{k_t} = B_i^{k_t} \quad i=1\cdots N_p \tag{202}$$

where

$$A_{ij}^{k_t} = -\frac{1}{2}\delta(i,j) + I_{s0ij} + \delta_L(l,j)I_{L0il} \tag{203}$$

and

$$\begin{aligned} B_i^{k_t} \;=\; & b_i^{k_t} - \Delta t[\frac{1}{2}\sum_{j=1}^{N_p}(\sigma_J)_j^0 I_{sfij}^{k_t} + \sum_{k=1}^{k_t-1}\sum_{j=1}^{N_p}(\sigma_J)_j^k I_{sfij}^{k_t-k}] \\ & -\Delta t[\frac{1}{2}\sum_{l=1}^{N_l}(\sigma_J)_l^0 I_{Lfij}^{k_t} + \sum_{k=1}^{k_t-1}\sum_{l=1}^{N_l}(\sigma_J)_l^k I_{Lfij}^{k_t-k}] \end{aligned} \tag{204}$$

in which

$$\delta_L(l,j) = \begin{cases} 1 \text{ when waterline segment } l \text{ is on panel } j \\ 0 \text{ when waterline segment } l \text{ is not on panel } j \end{cases} \tag{205}$$

and

$$b_i^{k_t} = \sqrt{\frac{\bar{a}L}{\pi g}}e^{-\bar{a}(k_t\Delta t)^2}(n_J)_i - \frac{1}{2}\sqrt{\frac{L}{g}}[1+\mathrm{erf}(\bar{a}k_t\Delta t)](m_J)_i \tag{206}$$

Similarly, the numerical scheme for the diffracted wave potential can be devised.

Appendix D: Results of Roll Damping for Series 60 Hull

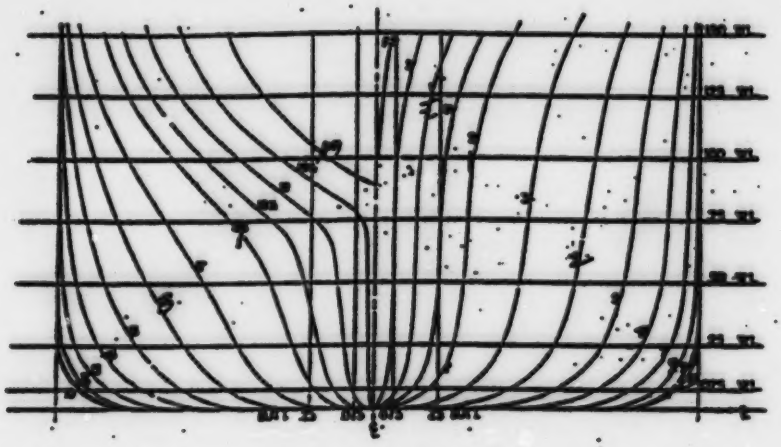

Figure 13: Body Plan of Series 60, C_B=0.70.

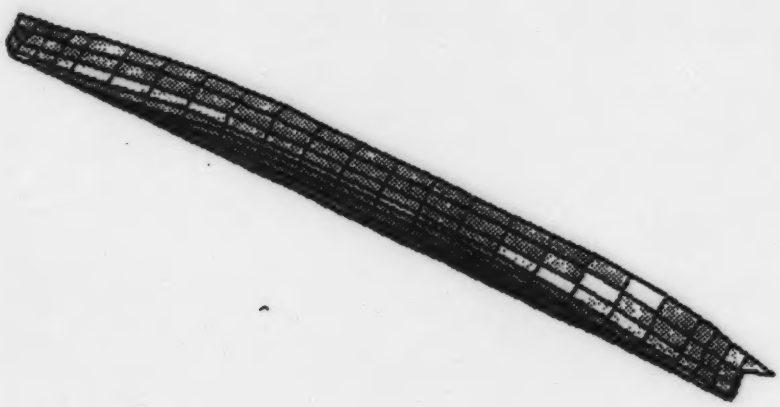

Figure 14: Panelized Hull of Series 60, C_B=0.70.

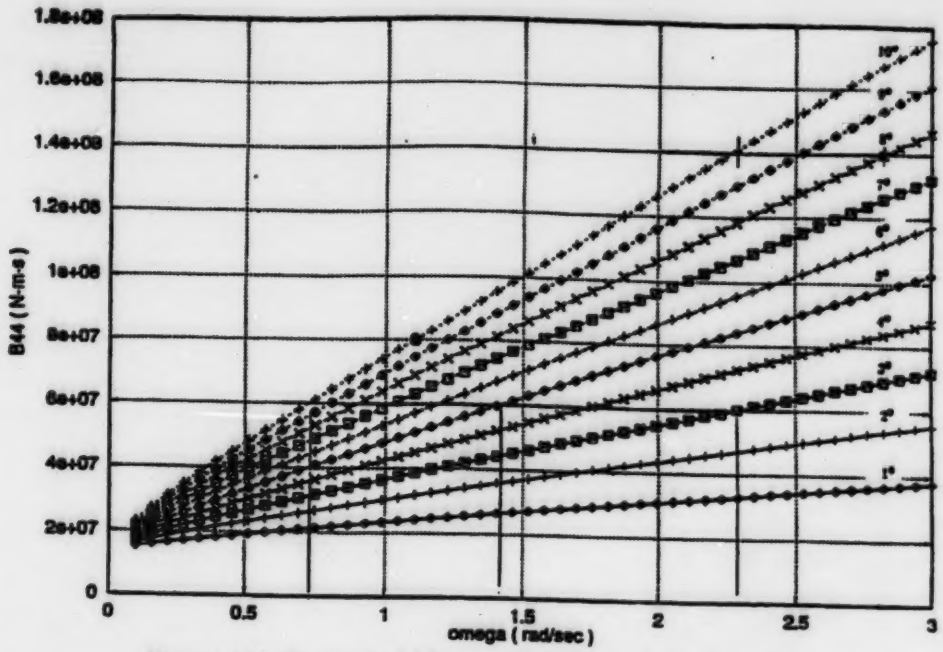

Figure 15: Computed Viscous Roll Damping, $F_n = 0.2$.

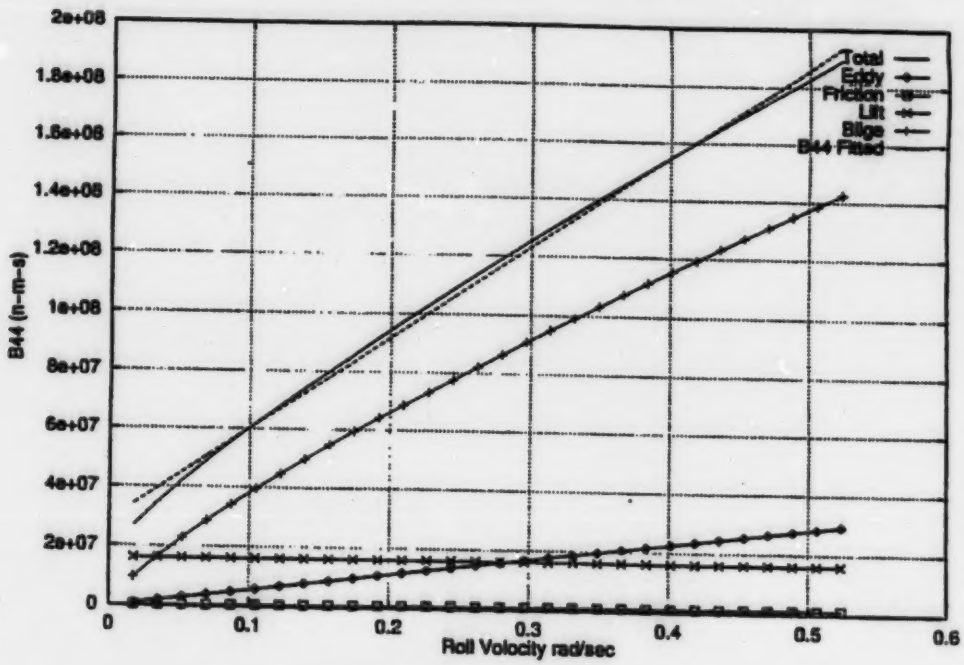

Figure 16: Fitted Roll Damping based on Fig.15.

Appendix E: Numerical Results

In the next phase of the project, thorough debugging and comprehensive validation of the code are to be undertaken. As a preliminary check, the proposed method has been used to compute the motions, pressures and sea loads of a frigate (CPF) with a constant forward speed in regular head waves. The results are presented in this appendix. The half-hull under the mean waterline is divided into 153 panels, see Fig.17. Numerical results given below are corresponding to the following conditions:
ship speeds: V_s=3.4, 8.2 and 12.0 knots (Froude numbers 0.05, 0.12 and 0.18);
wave steepness: H/λ=1/50;
ratio of wave and ship lengths: λ/L=1.19;
where H is the wave height, λ is the wave length, and the ship length L=124.5 m.

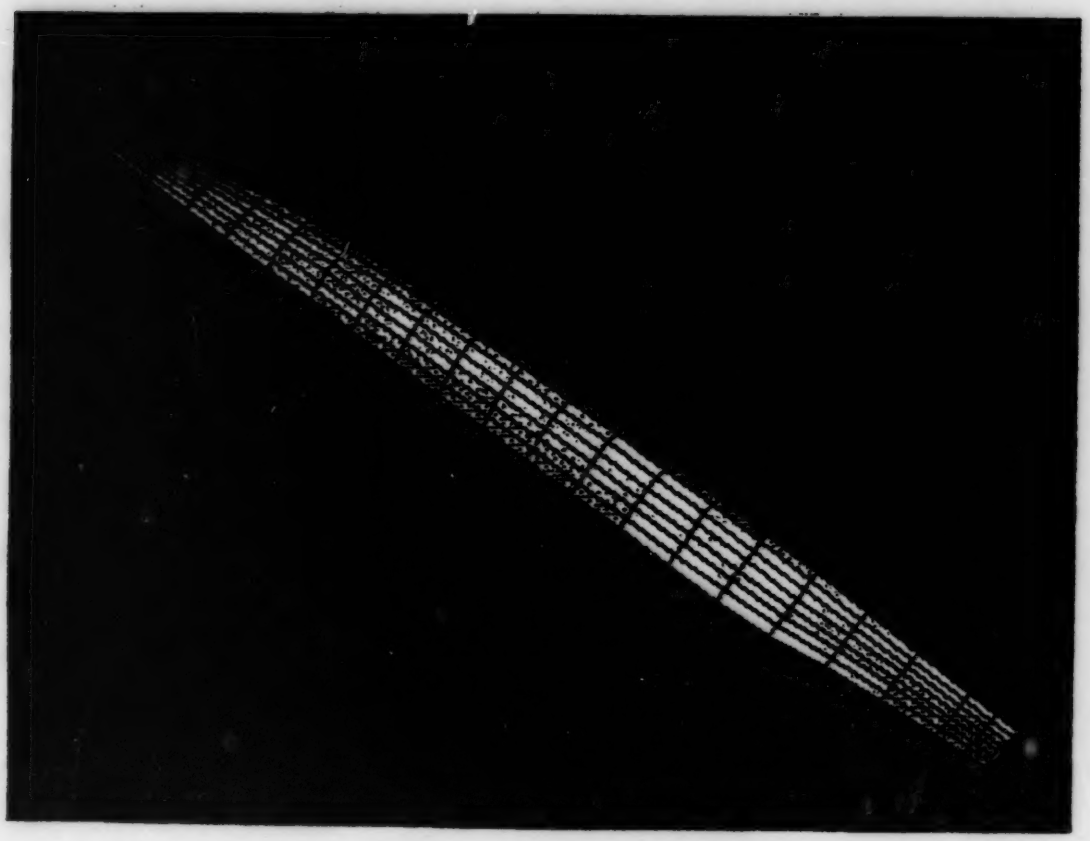

Figure 17: Panelization of CPF hull

Before validation of the computer code, the experimental data (Ando, 1999) were treated by a low-pass filter, because some high-frequencies exist, especially in the signals for pressure. Comparisons between the raw data and smoothed data are shown in Fig.18 through Fig. 20, where the solid lines denote the smoothed data, while the dashed lines denote the raw data.

The computed results for V_s=3.4 knots in regular head waves are shown in Fig.21 through Fig.22, compared with the corresponding experimental results. Henceforth, in all figures the computed results are expressed by the solid lines, while the data are displayed by the dashed lines. The input wave, the predicted heave and pitch of ship, and the sealoads on the midship section for the present method are shown in Fig.21. The predicted heave is in a good agreement with the experimental results, while the pitch is somewhat overestimated. The comparisons between the computed and measured pressures are shown in Fig.22. The agreement of the pressures over the forebody is reasonably good, while the discrepancy of the pressures for the points in the midbody and aftbody is significant. Further work has to be carried out to improve the computation of pressure over the whole hull.

Similarly, the comparisons between the computed and experimental results for V_s=8.2 knots are shown in Fig.23 and Fig.24, while the comparisons for V_s=12 knots are shown in Fig.25 and Fig.26, respectively. Generally speaking, the predicted motions, heave and pitch, agree well with the experimental counterparts. For the comparisons of pressures, agreement is good for points at the forebody and bad for points at the midship and aftbody; the comparisons for the sealoads are reasonably good. The agreement between experimental and computed results for the ship advancing at low speed is better than those at high speed.

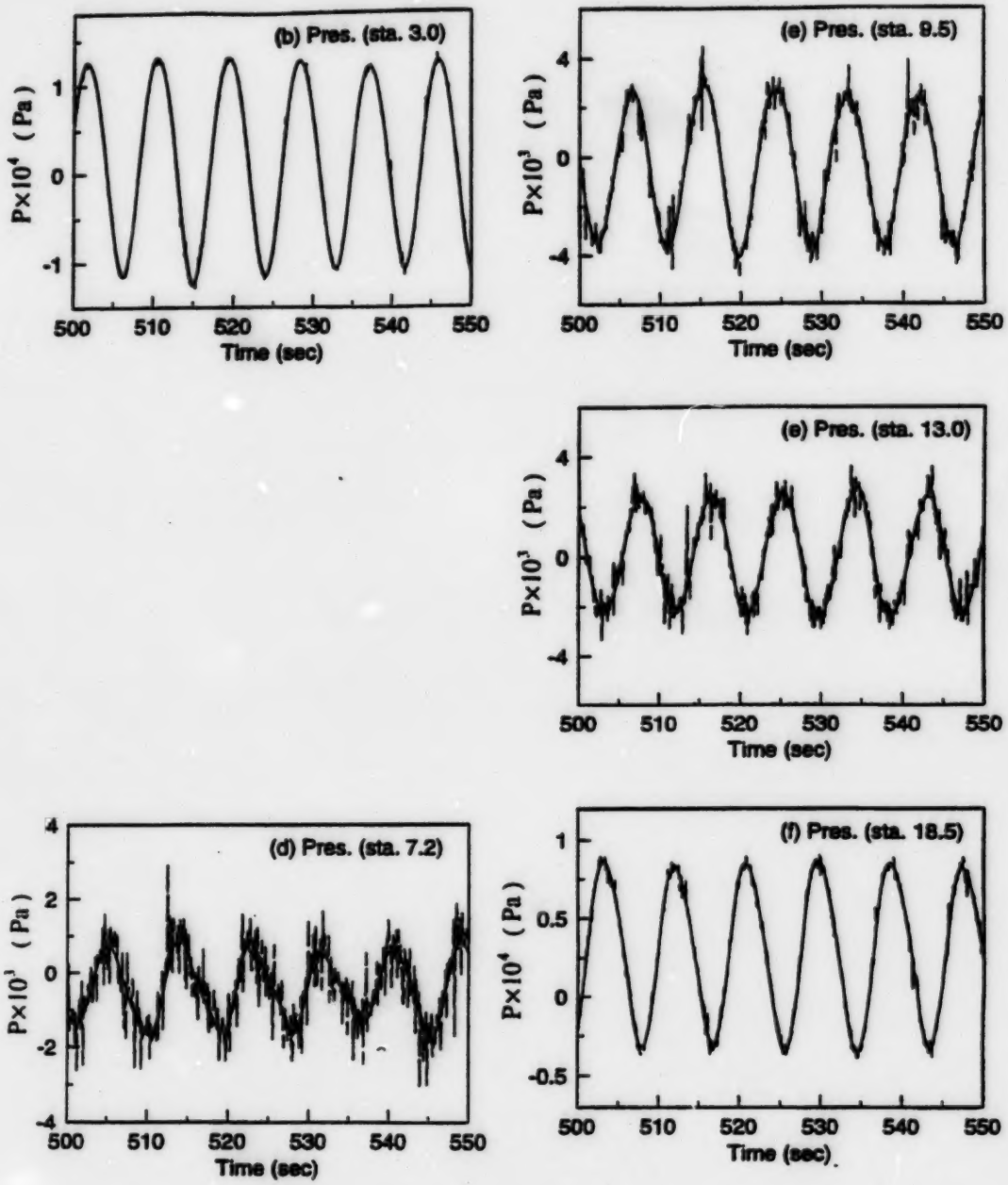

Figure 18: Raw and Smoothed Data of Pressure of CPF model (V_s=3.4 knot)

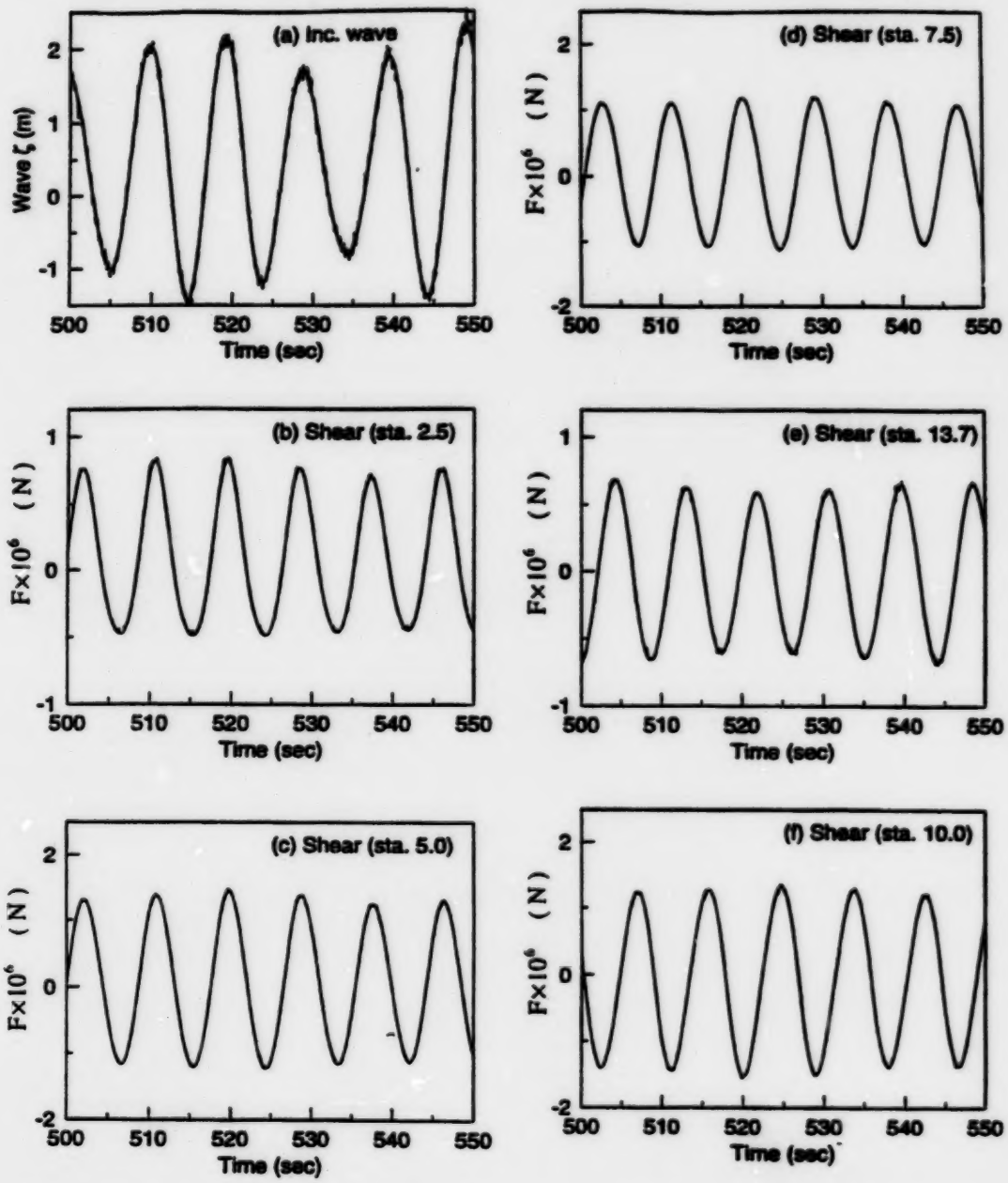

Figure 19: Raw and Smoothed Data of Shear Force of CPF model (V_s=3.4 knot)

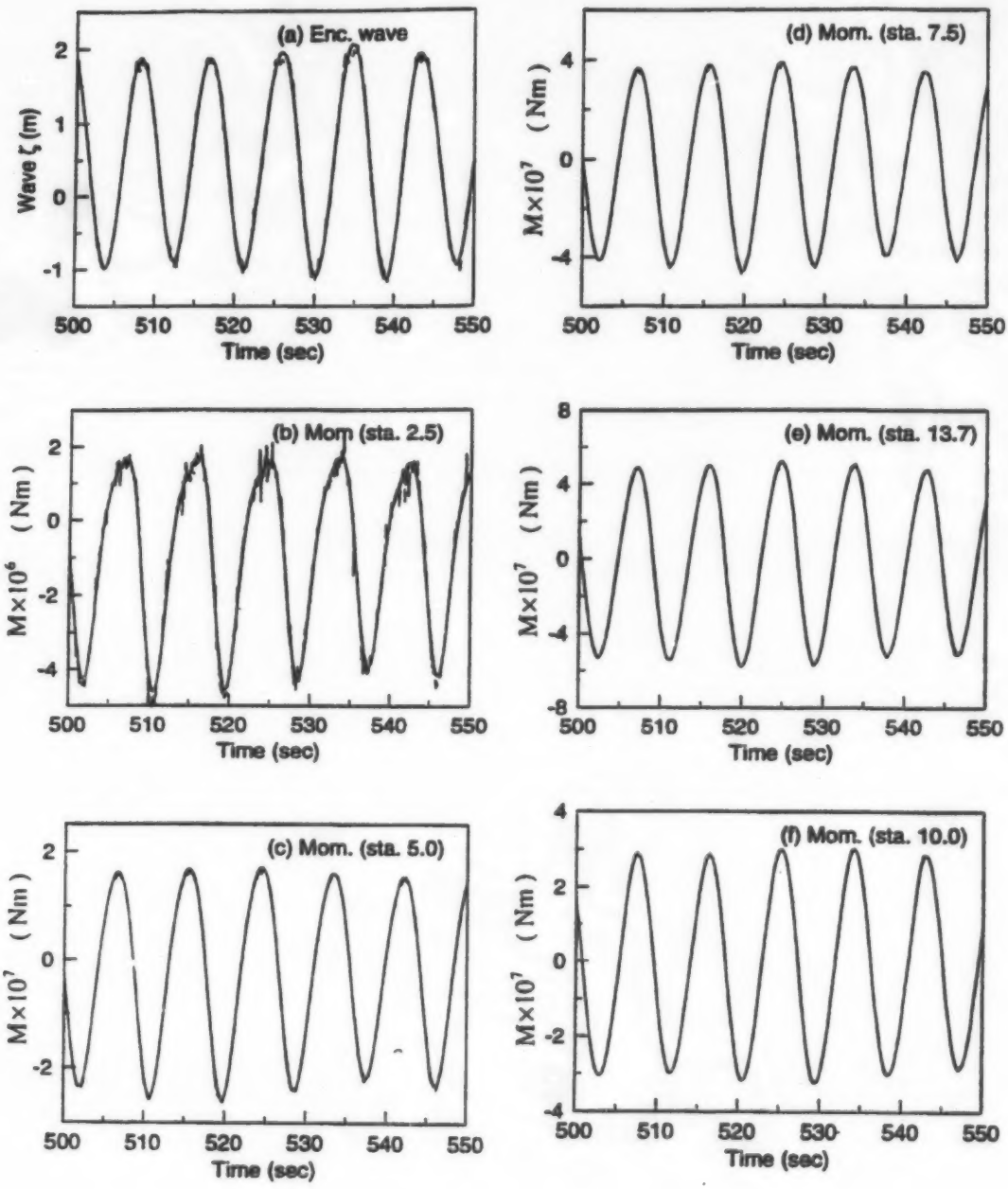

Figure 20: Raw and Smoothed Data of Bending Moment of CPF model (V_s=3.4 knot)

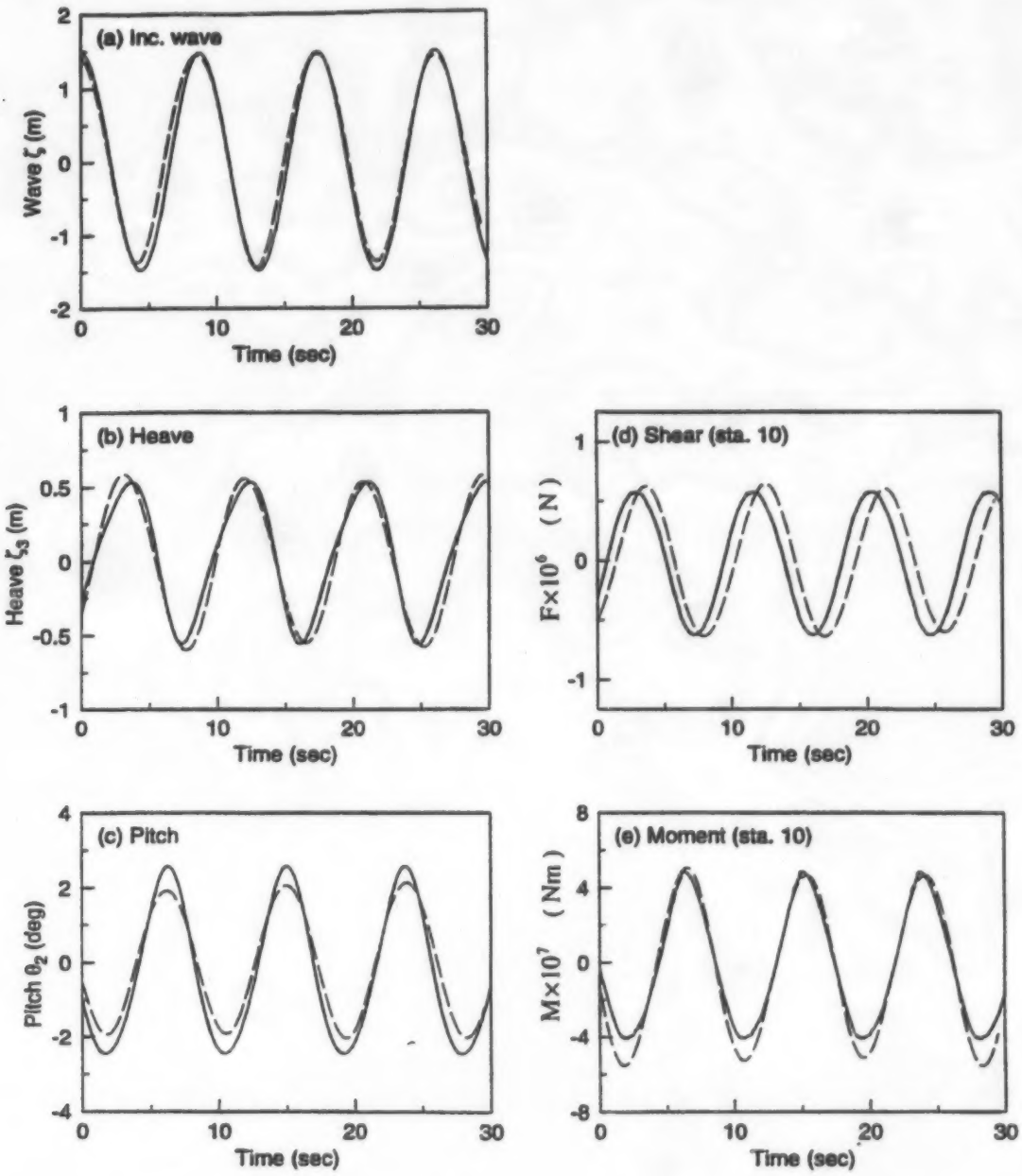

Figure 21: Wave, Motions and Sealoads of CPF at V_s=3.4 knot (— SEALOADS - - - Experiment)

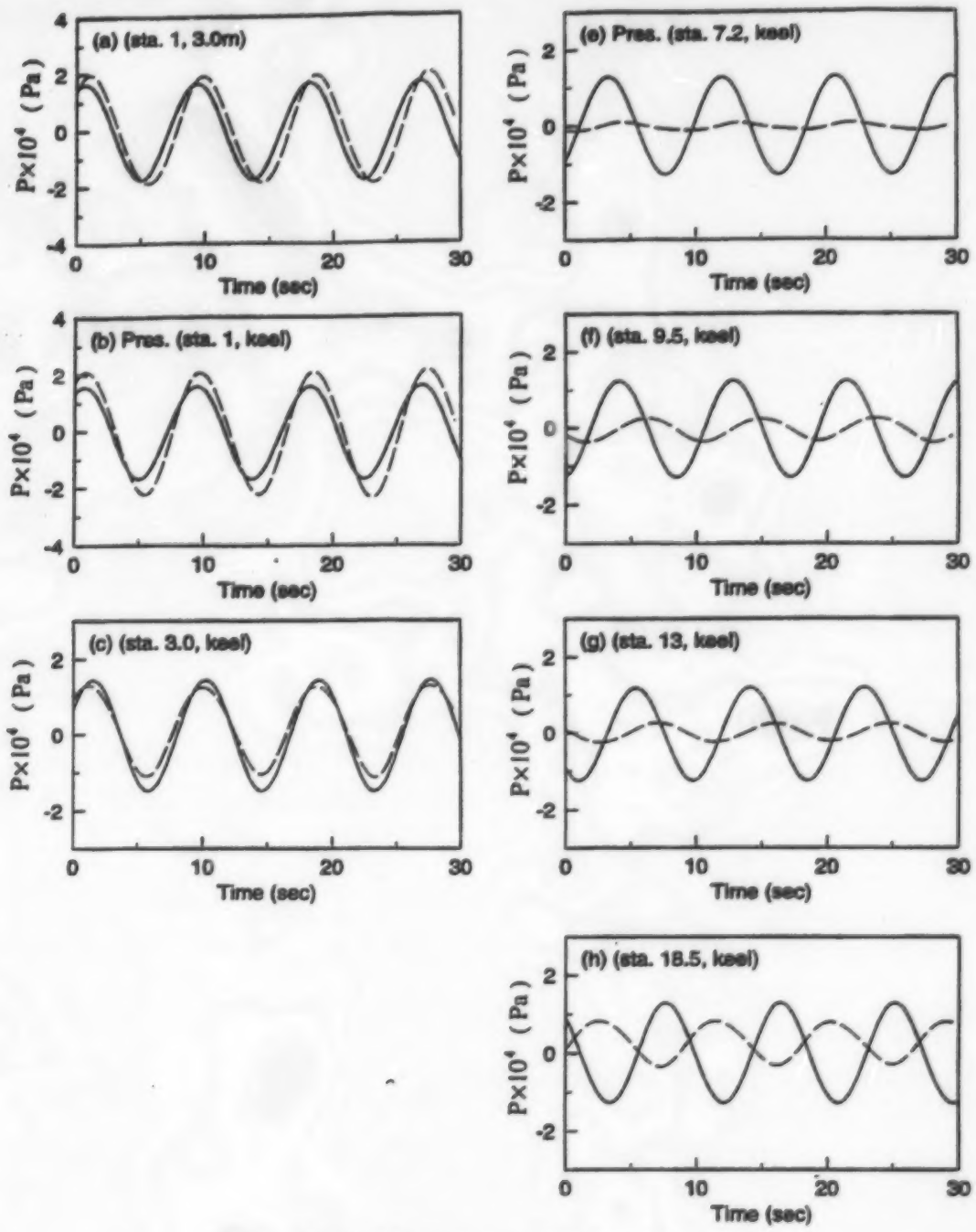

Figure 22: Hull Pressure on CPF (V_s=3.4 knot)

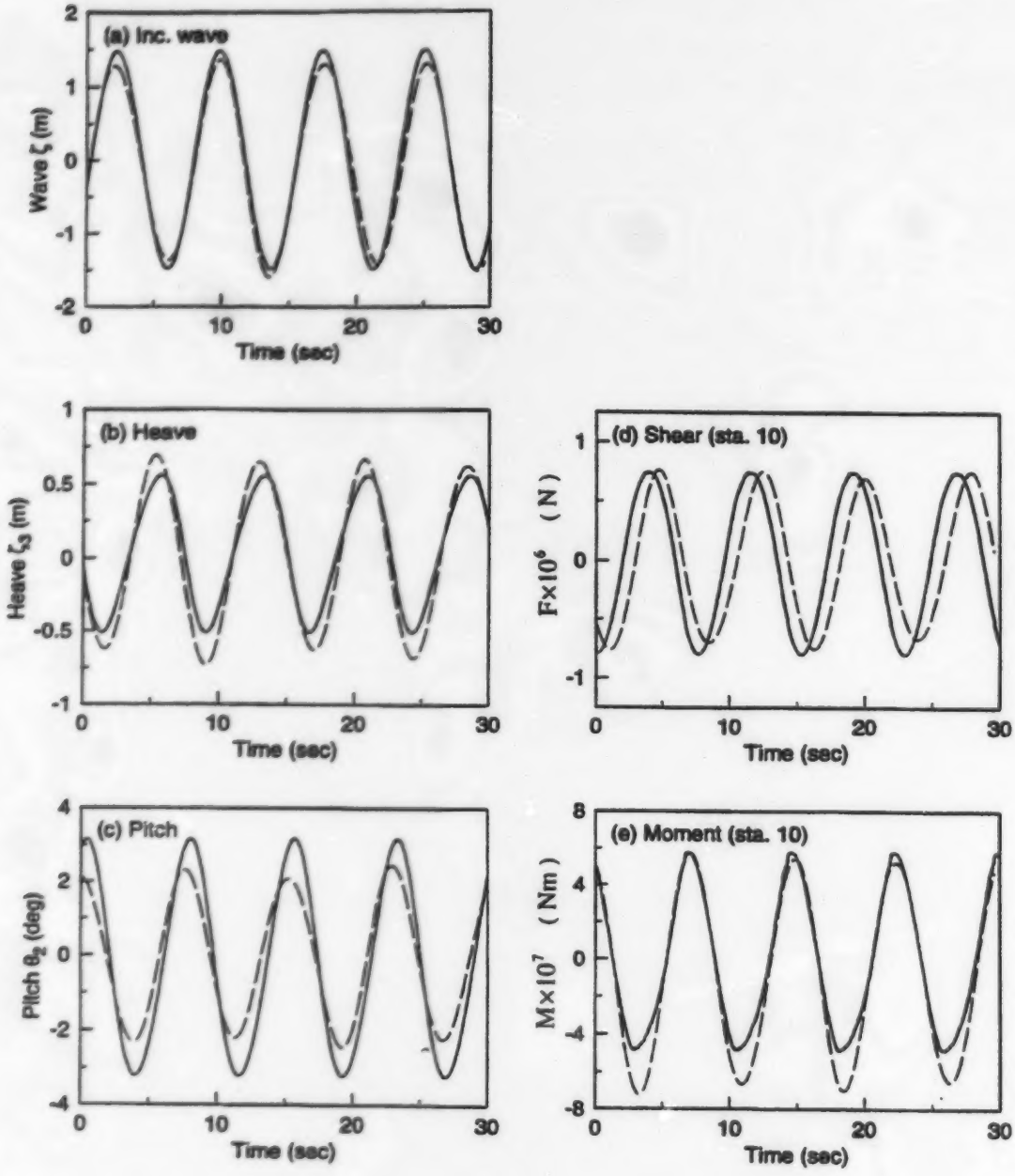

Figure 23: Wave, Motions and Sealoads of CPF (V_s=8.2 knot)

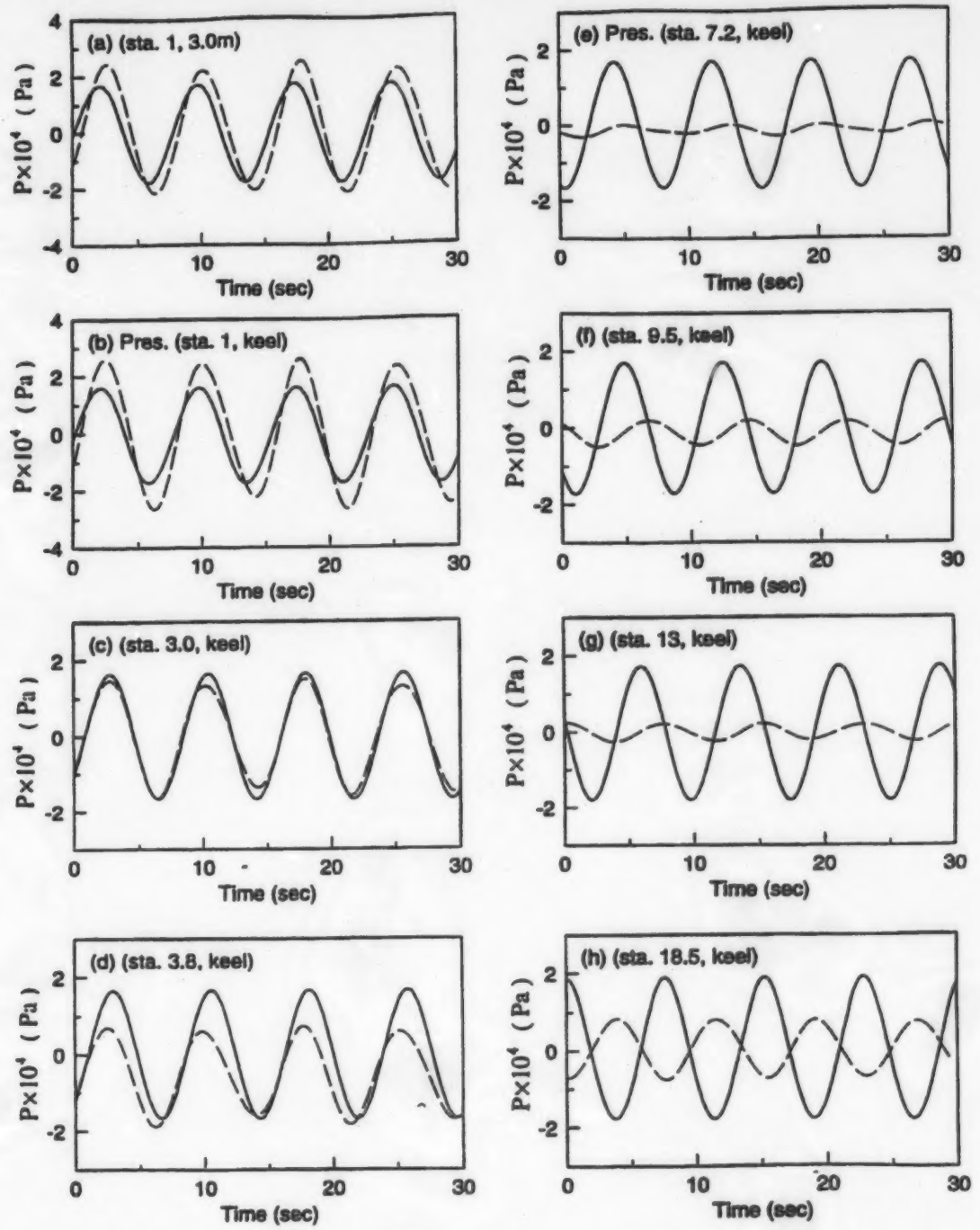

Figure 24: Hull Pressure on CPF (V_s=8.2 knot)

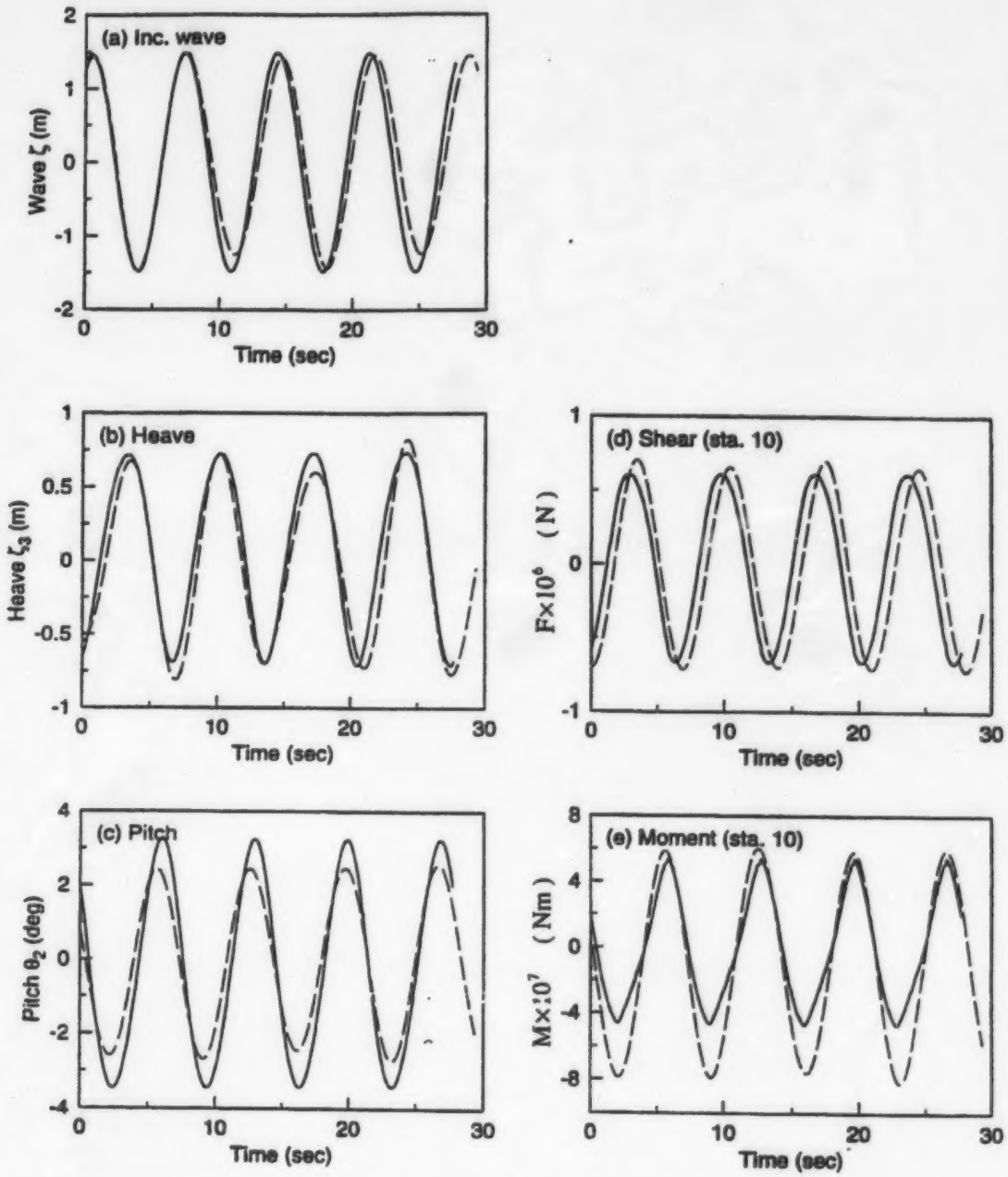

Figure 25: Wave, Motions and Sealoads of CPF (V_s=12 knot)

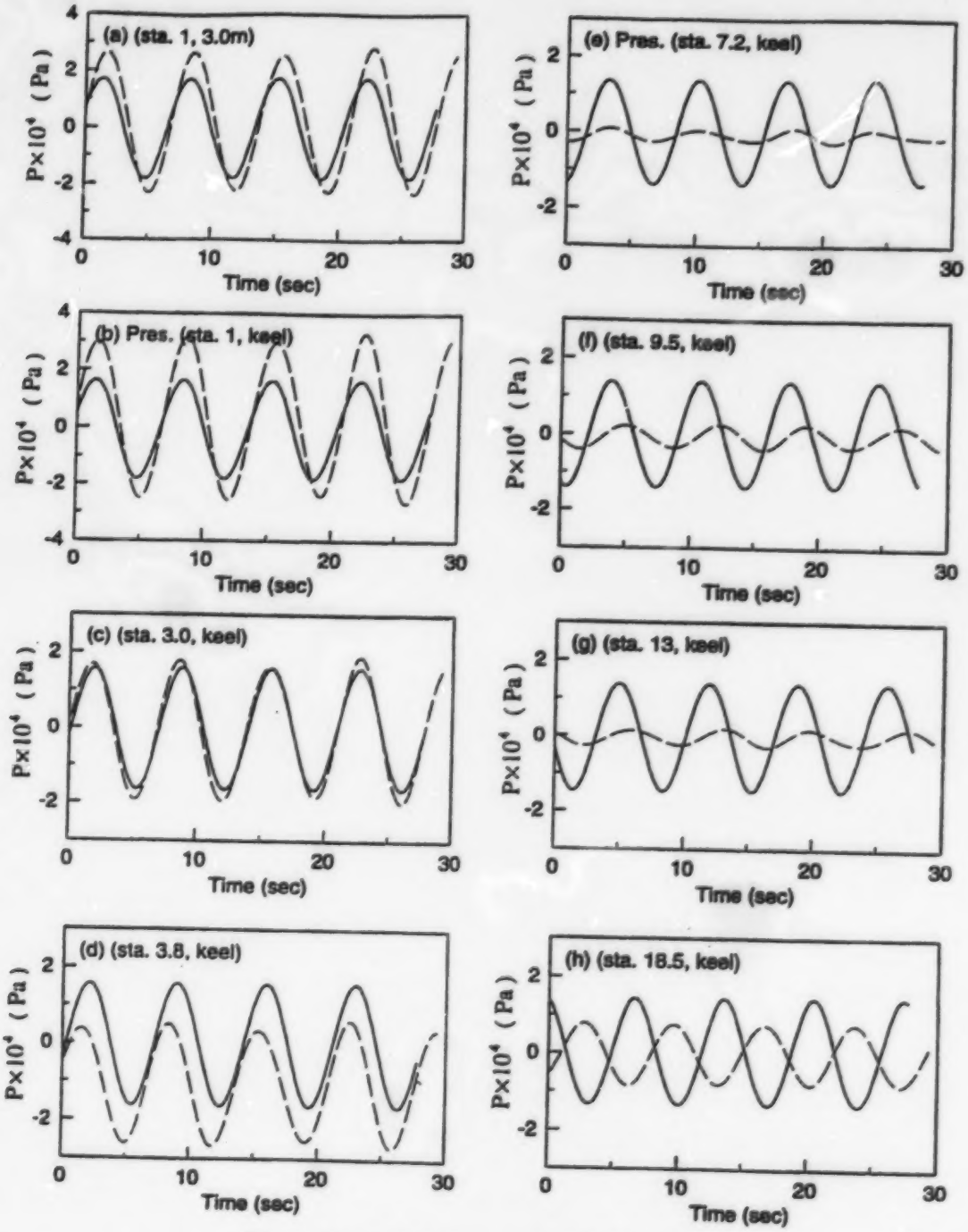

Figure 26: Hull Pressure on CPF (V_s=12 knot)

References

Abramowitz, M. and Stegun, I. A.(1964). Handbook of Mathematical Functions. National Bureau of Standards, Washington, D. C.

Ando, S.(1999). Wave-Induced Motions, Loads, and Hydrodynamic Pressures on a Model Frigate, DREA Technical Memorandum, in preparation.

Ando, S. and Cumming, D.C., (1991). Head-Wave Diffraction by a Slender Ship. International Shipbuilding Progress, Vol. 38, No. 414, 99-113.

Barakat, R. (1962). Vertical Motion of a Floating Sphere in a Sine-wave Sea. Journal of Fluid Mechanics, Vol. 13, 540-556. Beck, R. F. and King, B. (1989). Time-Domain Analysis of Wave Exciting Forces on Floating Bodies at Zero Forward Speed. Applied Ocean Research, Vol. 11, 19-25.

Beck, R. F. and Liapis, S. J. (1987). Transient Motion of Floating Bodies at Zero Forward Speed. Journal of Ship Research, Vol. 31, 164-176.

Beck, R. F. and Magee, A. (1990). Time-Domain Analysis for Predicting Ship Motions. Proceedings of IUTAM Symposium, Dynamics of Marine Vehicles and Structures in Waves, London.

Bingham, H. B., Korsmeyer, F. T., Newman, J. N. and Osborne, G. E. (1993). The Simulation of Ship Motions, Proceedings of the 6th International Conference on Numerical Ship Hydrodynamics. Iowa City, USA.

Cummins, W. E. (1962). The Impulse Response Function and Ship Motions, Schiffstechnik, Vol. 9, 101-109.

de Kat, Jan O. (1990). The Numerical Modeling of Ship Motions and Capsizing in Servere Seas, Journal of Ship Research, Vol. 34, 289-301.

de Kat, Jan O. and Paulling, J. R. (1989). The Simulation of Ship Motions and Capsizing in Servere Seas. Transactions of SNAME, Vol. 97, 139-168.

de Kat, J.O., Brouwer, R., McTaggart, K. A. and Thomas, W. L. (1994). Intact Ship Survivability in Extreme Waves: New Criteria from a Research and Navy Perspective. STAB'94, Florida.

Finklestein, A. (1957). The Initial Value Problem for Transient Water Waves. Communications on Pure and Applied Mathematics, Vol. 10, 511-522.

Hess, J. L. and Smith, A. M. O. (1967). Calaulation of Potential Flow about Arbitrary Bodies. Progress in Aeronautical Science, Vol. 8, 1-38.

Holtrop, J. and Mennen, G. G. J. (1982). An Approximate Power Prediction Method.

International Ship Building Progress, No. 335, Vol. 29.

Hsiung, C. C. and Huang, Z. J. (1991). Comparison of the Strip Theory and the Panel Method in Computing Ship Motion with Forward Speed. Proceedings of Symposium on Selected Topics of Marine Hydrodynamics, St. John's, Nfld.

Huang Z. J., Cong L. Z., Grochowalski S. and Hsiung C. C., (1998). Capsize Analysis for Ships with Water Shipping on and off the Deck. Proceedings of the 22nd Symposium on Naval Hydrodynamics, Washington, D.C., USA.

Huang, Z. J. and Hsiung, C. C. (1997). Dynamic Simulation of Capsizing for Fishing Vessels with water on deck. STAB'97, Varna, Bulgaria.

Huang, Z. J. and Hsiung, C. C. (1996). Nonlinear Shallow Water Flow on Deck Coupled with Ship Motion. The 21st Symposium on Naval Hydrodynamics, Trondheim, Norway.

Huang, Z. J. (1995). Nonlinear Shallow Water Flow on Deck and its Effect on Ship Motion. Ph. D. Thesis, Technical University of Nova Scotia.

Huang, Z. J. and Hsiung, C. C. (1993a). An Improved 3-D Panel Method to Compute m-Terms for Ship Motion. Procedings of the Second Canadian Marine Dynamics Conference, Vancouver, B.C.

Huang, Z. J. and Hsiung, C. C. (1993b). Development of a Hydro-Aero Model for Predicting Slamming Loads on a Ship Hull. Technical Report to the Department of National Defence, Defence Research Establishment Atlantic. Centre for Marine Vessel Design and Research, Technical University of Nova Scotia, Halifax, Nova Scotia.

Huang, Z. J. and Hsiung, C. C. (1991). A New Algorithm for the Three-Dimensional Time - Domain Green Function. Technical Report NA-91-2, Department of Mechanical Engineering, Technical University of Nova Scotia.

Kijima, K., Katsuno, T., Nakiri, Y. and Furukawa, Y. (1991). On the Maneuvering Performance of a Ship with the Parameter of Loading Condition. Journal of the Society of Naval Architects of Japan, Vol. 168, 141-148.

King, B. K. (1990). A Fast Numerical Solver for Large Amplitude Ship Motions Simulation. STAB'90, Naple, Spain.

King, B. K., Beck, R. F. and Magee, A.R. (1988). Seakeeping Calculations With Forward Speed Using Time Domain Analysis, Proceedings of the Seventeenth Symposium on Naval Hydrodynamics, The Hague, Netherland.

Liapis, S. and Beck, R. F. (1985). Seakeeping Computations Using Time Domain Analysis. Proceedings of the Fourth International Conference on Numerical Ship Hydrodynamics, Washington, D.C.

Lin, W. M. and Yue, D. K. (1994). Large Amplitude Motions and Wave Loads for Ship Design. Proceedings of the 20th Symposium on Naval Hydrodynamics, Santa Barbra, California.

Lin, W. M. and Yue, D. K. (1990). Numerical simulations for Large Amplitude Ship Motions in the Time Domain. Proceedings of the 18th Symposium on Naval Hydrodynamics, Ann Arbor, Michigan.

Luke, Y.L. (1962). Integral of Bessel Functions. McGraw-Hill Book Company,Inc. U.S.A.

Magee, A. (1994). Seakeeping Applications Using a Time-Domain Method. Proceedings of the 20th Symposium on Naval Hydrodynamics, Santa Barbra, California.

Nakos, D. E., Kring, D. and Sclavounos, P.D. (1993). Rankine Panel Methods for Transient Free Surface Flows. Proceedings of the 6th International Conference on Numerical Ship Hydrodynamics, Iowa City.

Newman, J. N. (1978). The Theory of Ship Motions. Advances in Applied Mechanics, Vol. 18, 222-283.

Ogilve, T. F. and Tuck, E. O. (1969). A Rational Strip Theory of Ship Motion: Part I. Department of Naval Architecture, The University of Michigan, Report No. 013, 1969.

Schmitke, R. T. (1978). Ship Sway, Roll and Yaw Motion in Oblique Seas. Transactions SNAME, Vol. 86.

van Oortmerssen, Gerard (1976). The Motion of a Moored Ship in Waves. NSMB Publication No. 510.

Waston, G.N. (1952). A treatise on the theory of Bessel Functions. Cambrige, University Press, U.K.

Wehausen J. V. (1967). Initial Value Problem for the motion in an Undulating Sea of a Body with Fixed Equilibrium Position. Journal of Engineering Mathematics, Vol. 1, 1-19.

Wehausen, J. V. and Laitone, E. V. (1960). Surface Waves. Handbuck der Physik, Springer-Verlag, Vol. 9.

Wu, G. X. (1991). A Numerical Scheme for Calculating the m_j-terms in Wave-Current-Body Interaction Problem. Applied Ocean Research, Vol. 13, 317-319.

UNCLASSIFIED
SECURITY CLASSIFICATION OF FORM
(highest classification of Title, Abstract, Keywords)

DOCUMENT CONTROL DATA

(Security classification of title, body of abstract and indexing annotation must be entered when the overall document is classified)

1. ORIGINATOR (the name and address of the organization preparing the document.. Organizations for whom the document was prepared, e.g. Establishment sponsoring a contractor's report, or tasking agency, are entered in section 8.)

Centre for Marine Vessel Development and Research
DalTech, Dalhousie University,
P.O. Box 1000, Halifax, NS B3J 2X4

2. SECURITY CLASSIFICATION (overall security classification of the document including special warning terms if applicable).

UNCLASSIFIED

3. TITLE (the complete document title as indicated on the title page. Its classification should be indicated by the appropriate abbreviation (S,C,R or U) in parentheses after the title).

Theoretical Manual for SEALOADS: A Three-Dimensional Nonlinear Time-Domain Sea Loads Computer Code

4. AUTHORS (Last name, first name, middle initial. If military, show rank, e.g. Doe, Maj. John E.)

Cong, Liangzi, Wei Qiu, and Hsiung, C.C.

5. DATE OF PUBLICATION (month and year of publication of document)	6a. NO .OF PAGES (total containing information Include Annexes, Appendices, etc).	6b. NO. OF REFS (total cited in document)
October 1999	x, 65	39

7. DESCRIPTIVE NOTES (the category of the document, e.g. technical report, technical note or memorandum. If appropriate, enter the type of report, e.g. interim, progress, summary, annual or final. Give the inclusive dates when a specific reporting period is covered).

CONTRACTOR REPORT

8. SPONSORING ACTIVITY (the name of the department project office or laboratory sponsoring the research and development. Include address).

Defence Research Establishment Atlantic
PO Box 1012
Dartmouth, NS, Canada B2Y 3Z7

9a. PROJECT OR GRANT NO. (if appropriate, the applicable research and development project or grant number under which the document was written. Please specify whether project or grant).	9b. CONTRACT NO. (if appropriate, the applicable number under which the document was written).
1gb13	W7707-7-4636

10a ORIGINATOR'S DOCUMENT NUMBER (the official document number by which the document is identified by the originating activity. This number must be unique to this document.)	10b OTHER DOCUMENT NOs. (Any other numbers which may be assigned this document either by the originator or by the sponsor.)
	DREA CR/98/443

11. DOCUMENT AVAILABILITY (any limitations on further dissemination of the document, other than those imposed by security classification)

(X) Unlimited distribution
( ) Defence departments and defence contractors; further distribution only as approved
( ) Defence departments and Canadian defence contractors; further distribution only as approved
( ) Government departments and agencies; further distribution only as approved
( ) Defence departments; further distribution only as approved
( ) Other (please specify):

12. DOCUMENT ANNOUNCEMENT (any limitation to the bibliographic announcement of this document. This will normally correspond to the Document Availability (11). However, where further distribution (beyond the audience specified in (11) is possible, a wider announcement audience may be selected).

UNCLASSIFIED
SECURITY CLASSIFICATION OF FORM

13. ABSTRACT (a brief and factual summary of the document. It may also appear elsewhere in the body of the document itself. It is highly desirable that the abstract of classified documents be unclassified. Each paragraph of the abstract shall begin with an indication of the security classification of the information in the paragraph (unless the document itself is unclassified) represented as (S), (C), (R), or (U). It is not necessary to include here abstracts in both official languages unless the text is bilingual).

This report describes the theoretical formulation for SEALOADS, a computer program for the time-domain prediction of ship motions, sea loads, and hydrodynamic pressures on a ship hull. The three-dimensional time-domain Green function is used to derive the forces due to radiated and diffracted waves. The Froude-Krylov forces are computed at the instantaneous position using the three-dimensional panel method. Nonlinear viscous damping, resistance, and cross-flow drag are included. The propeller thrust, rudder and maneuvering forces are also taken into account. After the nonlinear equations of ship motions are solved in the time domain, hydrodynamic pressures on the ship hull and bending moments and shear forces acting on a cross section of the ship are computed.

14. KEYWORDS, DESCRIPTORS or IDENTIFIERS (technically meaningful terms or short phrases that characterize a document and could be helpful in cataloguing the document. They should be selected so that no security classification is required. Identifiers, such as equipment model designation, trade name, military project code name, geographic location may also be included. If possible keywords should be selected from a published thesaurus. e.g. Thesaurus of Engineering and Scientific Terms (TEST) and that thesaurus-identified. If it not possible to select indexing terms which are Unclassified, the classification of each should be indicated as with the title).

ship motions
sea loads
hydrodynamic pressures
nonlinear forces
time domain
3-dimensional panel method
computer program manual